



The alkali resistance of CuNbTi catalyst for selective reduction of NO by NH₃: A comparative investigation with VWTi catalyst

Xiaoxiang Wang^a, Qiliang Cong^a, Liang Chen^a, Yun Shi^b, Yao Shi^a, Sujing Li^{a,*}, Wei Li^{a,*}

^a Key Laboratory of Biomass Chemical Engineering of Ministry of Education, Institute of Industrial Ecology and Environment, College of Chemical and Biological Engineering, Zhejiang University, Hangzhou 310027, China

^b Zhejiang University of Science & Technology, Hangzhou 310023, China



ARTICLE INFO

Keywords:
CuNbTi catalyst
VWTi catalyst
NH₃-SCR
Alkali metal resistance
Synergistic effect

ABSTRACT

The alkali metal poisoned CuNbTi and VWTi catalysts were prepared by wetness impregnation method. Poisoning effects of various K₂O mass ratios (0.1%–2%) on CuNbTi and VWTi catalysts were studied, respectively. CuNbTi exhibited an excellent alkali metal resistance that 2%K₂O-CuNbTi still remained 80% NO_x conversion efficiency and 98% N₂ selectivity while 2%K₂O-VWTi was completely deactivated. Moreover, different alkali metals (K, Na, Ca, Mg) with the same molar ratio were doped on CuNbTi. The poisoned degree followed the order: K₂O > Na₂O > CaO > MgO. Then 2%K₂O-CuNbTi and 2%K₂O-VWTi were selected for follow-up study. To understand the poisoning mechanism, further investigations were performed by SEM, XRD, N₂-physisorption, XPS, EPR, NH₃-TPD, Py-IR, H₂-TPR, in situ DRIFTS characterizations and DFT calculations. The particle of CuNbTi and VWTi agglomerated and the surface area decreased after 2%K₂O loading. Loss of acid sites and drop of reducibility resulted in the deactivation of 2%K₂O-VWTi. By contrast, experimental and computational results indicated that the alkali resistance of 2%K₂O-CuNbTi was mainly due to the interaction between Ti₂NbO_x support and K atoms that K atoms were preferentially bound to Nb=OH and Nb=O with a lower bonding energy of $-2.33\text{ eV} - 2.83\text{ eV}$ when Cu atoms were coordinated to Ti=O with a binding energy of -1.54 eV . This protected the active copper species from linking to K₂O and the weak acid sites were preserved with the increasing isolated Cu²⁺. Ti₂NbO_x weakened the impact of potassium on NH₃ adsorbing over the catalyst while the preserved copper species provided adsorption sites and redox ability for NH₃-SCR reaction. Hence, the synergistic effect of copper and niobium species contributed to the alkali metal resistance. Ti₂NbO_x trapped the potassium and retained active copper species over 2%K₂O-CuNbTi catalyst while potassium deactivated both TiO₂ and active vanadium species on 2%K₂O-VWTi catalyst. Meanwhile, both Eley-Rideal (E-R) and Langmuir-Hinshelwood (H-L) mechanisms with adsorbed NH₃ coordinated to the Lewis acid sites and bidentate nitrate as the dominating intermediate species existed during the NH₃-SCR reaction procedure over 2%K₂O-CuNbTi at 225 °C.

1. Introduction

Nitrogen oxides (NO_x) in the air could cause a series of hazardous environmental pollution problems, such as acid rain, ozone depletion and photochemical smog etc. [1] Selective catalytic reduction of NO_x by NH₃ (NH₃-SCR) is one of efficient technologies for NO_x abatement [2] and the catalyst is the core of this technology. Different catalysts were developed for different applications, including stationary sources and mobile sources [3]. Especially, for the stationary sources, which included coal fired power plants, biomass combustion plants and solid-waste incineration plants, they would emit large amount of flue gas containing complex components, such as NO_x, SO_x, alkaline metals

[1,4]. However, alkaline earth metals of potassium (K), sodium (Na), magnesium (Mg) and calcium (Ca) in the flue gas could deactivate the SCR catalysts seriously [5]. Therefore, the effect of alkali metals on the SCR catalyst must be taken into consideration in NH₃-SCR catalytic research.

The poisoning effects of alkali on the SCR catalysts have been extensively investigated. Most scholars have studied the influence of alkali metals on traditional VW(Mo)Ti catalysts. Chen [6] proposed that the poisoning degree of different alkali metals on the V₂O₅-WO₃/TiO₂ was K > Na > Mg. Tang [7] suggested that sodium coordinated with vanadia species and decreased the acid sites and reducibility of V₂O₅/TiO₂. Li et al. [8] compared the effects of different calcium salts on the

* Corresponding authors.

E-mail addresses: sujing-li@zju.edu.cn (S. Li), w_li@zju.edu.cn (W. Li).

V_2O_5 - WO_3 / TiO_2 catalyst and found that the $CaCO_3$ poisoned catalyst showed the lowest activity while $CaSO_4$ had the slightest influence. Kröcher [9] found that the acid sites were blocked by additive alkali metals occupying the non-atomic V_2O_5 (010) sites, resulting in a strong deactivation of V_2O_5 - WO_3 / TiO_2 catalyst. Besides, the alkali metal poisoned Ce-Ti catalyst was learned by Du [10]. Experimental and theoretical results showed that the interaction of alkali metal atom with oxygen of CeO_2 and TiO_2 led to a deactivation. Fehrman [11] compared the alkali resistance under different amount of copper doping on Cu/zeolite catalyst and optimized the content of copper species. At present, the deactivation by alkali metal was correlated to the drop of acid sites and reducibility of active species.

$CuNbTi$ catalyst was proved to have a remarkable NO_x conversion efficiency from our previous investigation [12]. However, its alkali resistance has not been studied. In this paper, we compared the poisoning effects of different alkali metals on $CuNbTi$ catalyst. Commercial V_2O_5 - WO_3 / TiO_2 catalyst was also studied for comparison. And $CuNbTi$ catalyst was found to exhibit a better anti-alkali property than VWTi catalyst in this work. Meanwhile, different alkali resistance and poisoning mechanisms between $CuNbTi$ and VWTi catalysts under the same conditions were explored.

2. Experimental

2.1. Catalysts synthesis

The 0.8%Cu/ Ti_2NbO_x catalyst was prepared by co-precipitation and wetness impregnation methods, which were described in detail in our previous publication [12]. The V_2O_5 - WO_3 / TiO_2 catalyst with 1 wt% V_2O_5 and 5 wt% WO_3 doping was synthesized by impregnation method. Ammonium metavanadate and ammonium paratungstate as precursors were dissolved in oxalic acid solution and deionized water, respectively. And then both of the solutions were mixed in a desired proportion. The P25 titania nanoparticles (Degussa, $S_{BET} = 55m^2/g$, about 85% anatase and 15% rutile) were immersed in the mixture and kept in a rotary evaporator under 60 °C until water was removed. Afterwards, the prepared samples were dried at 110 °C for 8 h and calcined under 550 °C in air for 4 h. The 0.8%Cu/ Ti_2NbO_x catalyst was labeled as $CuNbTi$ while V_2O_5 - WO_3 / TiO_2 catalyst was denoted as VWTi for short hereafter.

The K_2O -doped $CuNbTi$ and VWTi catalysts with different mass ratio from 0.1 wt% to 2 wt% were also prepared by the incipient-wetness impregnating the $CuNbTi$ and VWTi catalysts with KNO_3 aqueous solution. The mixture was firstly dipped in an ultrasonic generator for 30 min and magnetic stirring for 4 h. The residue obtained was dried at 85 °C overnight, followed by calcining in the air at 550 °C for 4 h. Meanwhile, different alkali metal oxides (K, Na, Mg, Ca) were loaded on $CuNbTi$ catalysts with the same molar ratio by using the same method. $NaNO_3$, $Mg(NO_3)_2$ and $Ca(NO_3)_2$ were as the precursors. The poisoned catalysts were denoted as λM - $CuNbTi$ and λM -VWTi, which λ represented the weight percentage (0–2.5%) of the alkali metal oxides and M was K_2O , Na_2O , MgO and CaO , respectively. All the samples were ground and sieved to 40–60 mesh for the performance evaluation.

2.2. SCR activity measurements

The steady-state NH_3 -SCR measurements were performed in a fixed-bed quartz tube reactor (inner diameter = 6 mm) with the outflow gases monitored by Nicolet iS50 FTIR spectrometer. The typical feed gas consisted of 500 ppm NH_3 , 500 ppm NO, 5 vol% O_2 , 5%–10% H_2O (when used), 50–250 ppm SO_2 (when used) and N_2 as the balanced gas, with a total flow rate of 500 ml/min and a space velocity (GHSV) of 177,000 h⁻¹. The SCR reaction was carried out between 175 °C and 500 °C under atmospheric pressure and the quartz tube was heated by a temperature-controlled furnace. About 0.15 g catalysts of 40–60 mesh were loaded between plugs of glass wool in the quartz tube and a K-type

thermocouple was inserted to the catalyst bed to measure the reaction temperature. The effluent gas was kept throughout a heated gas cell (Pike Technologies, optical path length = 2.4 m), which was maintained at 110 °C during FTIR analysis. Initially the sample was activated with 10% O_2 / N_2 at 500 °C for 30 min to remove any possible adsorbed impurities and moisture. Afterwards, the catalyst was cooled down to room temperature and the reaction gas mixture was fed into the reactor. Each temperature was lasted 30 min for a steady state condition before collecting the spectrometer. The NO_x (NO and NO_2) conversion and N_2 selectivity were determined as follows:

$$NO_x \text{ conversion} = \frac{C_{NO_x(\text{in})} - C_{NO_x(\text{out})}}{C_{NO_x(\text{in})}} \times 100\% \quad (1)$$

$$C_{NO_x} = C_{NO} + C_{NO_2} + 2C_{N_2O} \quad (2)$$

$$N_2 \text{ selectivity} = (1 - \frac{2 \times C_{N_2O}}{C_{NO_x(\text{in})} + C_{NH_3(\text{in})} - C_{NO(\text{out})} - C_{NO_2(\text{out})} - C_{NH_3(\text{out})}}) \times 100\% \quad (3)$$

2.3. Catalyst characterization

The surface morphology and structure of the catalyst were studied with a scanning electron microscopy S4800 at 15kv. N_2 adsorption-desorption experiments were carried out by a Micromeritics 3Flex instrument to investigate the textural characteristics of different catalysts. And the BET surface area was calculated using Brunauer-Emmett-Teller (BET) method in the relative pressure (P/P_0) range of 0.05–0.30. X-ray diffraction (XRD) spectra were recorded at 0.02° intervals in the range of 10°–90° using X-ray diffractometer (PANalytical X' Pert PRO, Holland) equipped with a Cu-K α ($\lambda = 0.15406$ nm, 40kv and 40 mA) radiation. Meanwhile, the atomic chemical state of catalyst was analyzed by an X-ray photoelectron spectroscopy (XPS) on Thermo Scientific Escalab 250Xi instrument using Al K α ($h\nu = 1486.6$ eV) with a lower 10^{-7} pa base pressure. The pass energy was 30 eV and the catalyst was outgassed at room temperature before each test. Meanwhile, the obtained spectra were calibrated and standardized by carbon deposit C1 s peak at 284.6 eV. Electron paramagnetic resonance (EPR) spectra were determined using a Bruker A300 EPR Spectrometer with 0.2 mW microwave power in 110 K. Powder sample (about 20 mg) was contained in a quartz tube (OD = 1.5 mm) in each experiment. The center field was 3400 G and sweep width was 3000 G.

NH_3 temperature programmed desorption (NH_3 -TPD) experiments and temperature programmed reduction of hydrogen (H_2 -TPR) experiments were carried out on Micromeritics AutoChem II 2920. Prior to each experiment, 30 mg catalyst was placed in a quartz tube reactor and pretreated at 350 °C in a flow of high purified Helium (30 ml/min) for 1 h. Then the catalysts were cooled down to the room temperature in a flow of Helium. During each NH_3 -TPD experiment, the temperature was increased from 100 °C to 900 °C at a rate of 10 °C/min in Helium (30 ml/min) after reaching adsorption equilibrium in 10% NH_3 / He (30 ml/min) and purging with Helium for 2 h at 100 °C. The desorbed NH_3 signals were recorded by a quadrupole mass spectrometer (QIC-20). For the H_2 -TPR experiment, the sample was reduced in a mixture of 10% H_2 / Ar (30 ml/min) with the temperature increasing from 50 °C to 900 °C at a rate of 10 °C/min. And the signal was continuously monitored using a thermal conductivity detector (TCD) while the cold trap was used for eliminating the interference of H_2O .

Pyridine adsorption infrared spectrum (Py-IR) were conducted using a Nicolet infrared spectrometer by accumulating 4000 scans with a resolution of 0.4 cm⁻¹. The powder sample (about 10 mg) was pressed into a thin sheet and fixed into the sample cell. Then it was pretreated at 350 °C for 2 h under evacuation at a pressure of 1×10^3 Pa. The pyridine was adsorbed at the room temperature followed by a temperature-programming to 200 °C and maintaining 30 min. The infrared spectra were collected after the sample was cooled down to the room

temperature.

In-situ diffuse reflectance infrared Fourier transform spectroscopy (in situ DRIFTS) was collected in the range of 4000–650 cm^{−1} on a Fourier transform infrared spectrometer (FTIR, Nicolet NEXUS 6700) equipped with a Harrick IR cell and an MCT/A detector cooled by liquid nitrogen. The spectral resolution was 4 cm^{−1} with co-addition 64 scans. Before each test, the catalyst was heated up to 350 °C for 30 min in a flow of N₂ to remove adsorbed impurities. The background in each target temperature was collected in the cooling process.

2.4. Theoretical calculation

All the theoretical calculations were based on the density functional theory (DFT). The potassium atom was selected as a probe to be located on the surface of CuNbTi catalyst for further elucidating the effect of alkali metal. And all the spin polarized calculations were carried out on the Vienna ab initio simulation package (VASP) [13] with the version of 5.4.1, which was a plane wave density functional code. For each calculation, the electron-electron exchange and correlation interactions were described by using the generalized gradient approximation (GGA) with the form of the Perdew-Burke-Ernzerhof (PBE) [14] functional. The projector augmented wave (PAW) [15] method was employed to describe the interaction between the core and valence electrons. The plane-waves basis was set with a cutoff energy of 400 eV. And the convergence criteria for the electronic self-consistent iteration and the ionic relaxation loop were set as the values of 1 × 10^{−5} eV and 1 × 10^{−4} eV/Å, respectively. Brillouin zone integrations were performed with k-point sampling using Monkhorst-Pack(MP) [16] of 3 × 3 × 1 for the models. The method of Gaussian smearing was employed to determine the valence electrons occupancies with a smearing width of 0.05 eV.

As the (101) crystallographic plane was preferred to expose in the CuNbTi catalyst, which has been proved in our previous work [12]. Anatase-TiO₂ (101) and anatase-Ti₂NbO_x (101) surface with 4 atomic layers (two metal layers and two oxygen layers) of p (3 × 1) cell slab were prepared and cleaved, respectively. One thirds of titanium atoms were replaced by the niobium atoms in the model of Ti₂NbO_x support. The bottom two layers were fixed while the rest of two layers were fully relaxed. The dopant Nb were randomly distributed in the slab models. And the O-terminated surfaces were chosen and hydrogen-saturated because the massive OH groups were proved to exist in the results of FTIR (3.2.3 and 3.3). All the slabs models had the same vacuum space of more than 15 Å, which was large enough to avoid the interaction between periodical images.

The bonding energies (E_{B-Cu} , E_{B-K} and E_{B-NH_3}) were employed to evaluate the suitable site for Cu loading, K poisoning and NH₃ adsorption. They were calculated as following expression:

$$E_{B-Cu or B-K or B-NH_3} = E_{total} - E_{slab} - \frac{1}{n}E_{bulk-Cu or bulk-K or bulk-NH_3} \quad (4)$$

Where E_{total} was the total energy of the combined system with adsorbate copper loading on Ti₂NbO_x or TiO₂ supporting slab, potassium atoms binding to the CuNbTi or CuTi catalyst slab and NH₃ molecules adsorbing over CuTi or CuNbTi or KCuNbTi catalyst slab. And E_{slab} was the energy of slab before metal doping or NH₃ adsorbing. Meanwhile, $E_{bulk-Cu or bulk-K or bulk-NH_3}$ was the energy of bulk Cu or bulk K or bulk NH₃ (Cu = 4, K = 2 and NH₃ = 1). In the K poisoning process, -OH group was also one of possible site, and it would be transformed to -OK group under K existence. Under this situation, the bonding energies were calculated as follows:

$$E_{B-K} = E_{total} - E_{slab} - \frac{1}{n}E_{bulk-K} + \frac{1}{2}E_{H_2} \quad (5)$$

Note that the adsorption energy was a negative value as the exothermic adsorption and the smaller value indicated a strong interaction between the adsorption substrate and adsorbate [17].

The rigorous energy convergence threshold with the value of 10^{−7}

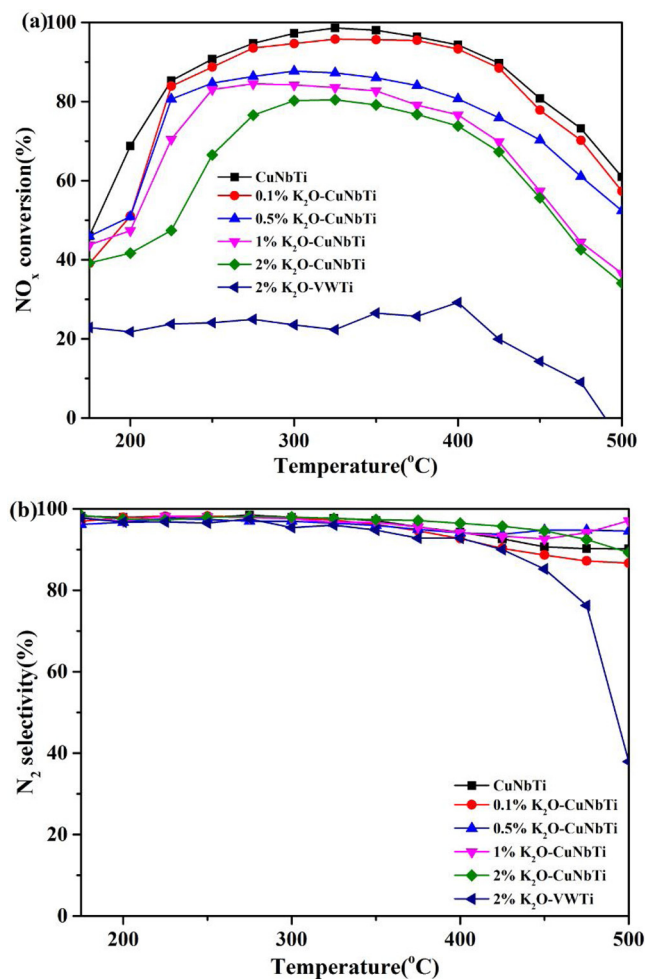


Fig. 1. NO_x conversion and N₂ selectivity over: (a)–(b) different mass ratios of K₂O-loaded CuNbTi and VWTi catalysts and (c)–(d) different alkalis poisoning CuNbTi catalysts. Reaction conditions: [NH₃] = [NO_x] = 500 ppm, [O₂] = 5%, [H₂O] = 5%, total flow rate = 500 mL min^{−1}, GHSV = 177,000 h^{−1} and N₂ as balance.

eV/unit cell was employed in vibrational calculations. Only surface O and OH were treated with 3 N degrees of freedom while the rest of the alloy surface was fixed during the vibrational calculations. All vibrations were treated as harmonic oscillator approximations.

3. Results and discussions

3.1. Catalytic activities

3.1.1. Influence of K₂O on NH₃-SCR activity of CuNbTi and VWTi catalysts

The DeNO_x activities of K₂O-CuNbTi catalysts with different amount of K₂O doping were reported in Fig. 1(a) and (b) as a function of reaction temperatures. 5% H₂O was introduced in the feed stream within the whole reaction temperature for simulating the real exhaust condition. The SCR activity decreased gradually with the increase of K₂O. 0.1%–0.5% K₂O showed slight influences on the SCR activities between 250 °C and 400 °C. However, with 1% of K₂O loading, the NO_x conversion decreased to 82.69%–84.49% in the temperature range of 250–350 °C and the highest NO_x conversion decreased from 98.57% to 84.49%. Further increasing K₂O mass ratio to 2% resulted in a decrease of the highest NO_x conversion from 84.49% to 80.46%, with a volcano shape curve. Meanwhile, VWTi with 2% K₂O doping was synthesized for comparison. 2%K₂O-VWTi catalyst showed about 20% NO_x conversion within the entire reaction temperature range. This indicated

that traditional VWTi catalyst with 2% K₂O loading showed a considerable deactivation, which was consistent with previous researches [6]. As for N₂ selectivity, K₂O poisoning CuNbTi catalysts exhibited a stable trend, since the N₂ selectivity was kept above 90% and N₂O formation was only about 10 ppm over the whole reaction temperature range. However, the N₂ selectivity of 2%K₂O-VWTi decreased gradually from 97.49% to 37.91% within 175–500 °C, while N₂O production reached a highest value of 39 ppm. Notably, the experiment demonstrated that CuNbTi catalyst exhibited a great anti-K₂O poisoning performance comparing with traditional VWTi catalyst. Meanwhile, the catalytic performance of aforementioned catalysts was tested without 5%H₂O adding into the reaction mixture gas (as shown in Fig. 1S(a)–(b)). It showed that the extent of K₂O poisoning became serious with the increase of doping amount, which was consistent with above results.

3.1.2. Influence of different alkalis on NH₃-SCR performances of CuNbTi catalysts

The DeNO_x performances of different alkalis poisoned CuNbTi catalysts were also tested with 5%H₂O existing in the mixture gas and depicted in Fig. 1(c) and (d). The molar ratio of alkali atom over each catalyst was equal with potassium atom proportion in 2%K₂O-CuNbTi (0.42 mmol/g). The mass fraction was 1.32%, 2.38%, 1.66% and 2% over Na₂O-CuNbTi, CaO-CuNbTi, MgO-CuNbTi and K₂O-CuNbTi samples, respectively. Different alkali oxides resulted in different poisoning degrees on its NH₃-SCR activity. Addition of 1.66%MgO on the CuNbTi resulted in a decrease during the whole reaction temperature range, but more than 90% of NO_x conversion was reached within the temperature range of 275–400 °C. 2.38% CaO-CuNbTi catalyst had a highest conversion of 91.04% at 350 °C, and the reaction temperature window over 90% NO_x conversion shrunk to 325–400 °C. The presence of Na₂O in the CuNbTi catalyst led to an obvious decline that the highest NO_x conversion was only 82.39% at 325 °C. Meanwhile, Na₂O-CuNbTi showed a similar behavior with K₂O-CuNbTi on NO_x conversion. However, the activity of 1.32%Na₂O-CuNbTi was slightly higher than those of 2% K₂O-CuNbTi. The addition of alkali had little effect on the N₂ selectivity and the value decreased slightly in the high temperature (400 °C–500 °C). Based on above findings, the poisoning degree of different alkali oxides on CuNbTi followed the order: K₂O > Na₂O > CaO > MgO. And this result was identical when 5% H₂O was eliminated from the feed gas, as shown in Fig. 1S(c)–(d). Chen [6] proposed the similar observation about poisoning effects of different alkali oxides on traditional V₂O₅-WO₃/TiO₂ catalysts in their study. Also, Tang [7] investigated the effect of sodium and calcium ions over V₂O₅/TiO₂ catalyst while Du [10] studied the deactivation mechanism of sodium and calcium salts loading Ce/TiO₂ catalyst, both stating that the poisoning degree of sodium was severer than that of calcium. All of their investigations were consistent with our results. 2% K₂O showed the most serious deactivation among all of equal molar alkali doping CuNbTi samples. Hence, 2%K₂O-CuNbTi was selected for the following research and a comparison was made between 2%K₂O-CuNbTi and 2%K₂O-VWTi to present the different poisoning mechanisms.

3.1.3. The effect of H₂O and/or SO₂ on NH₃-SCR reaction

The effect of H₂O and SO₂ on the NH₃-SCR reaction was evaluated for further simulating the real exhaust condition. And the transient response experiments of H₂O and/or SO₂ were conducted over 2%K₂O-CuNbTi catalyst at 325 °C. As can be seen from Fig. 2(a), the NO_x conversion of 2% K₂O-CuNbTi catalyst was kept at about 74% before adding H₂O. When 5%H₂O was joined in the feed stream, the NO_x conversion was kept stable at about 76% and N₂ selectivity was maintained 96%. Then the ratio of water vapor increased to 10%, and the NO_x conversion and N₂ selectivity nearly maintained unchanged, indicating that the water vapor in flue gas did not result in any further poisoning for 2%K₂O-CuNbTi catalyst.

SO₂ in the flue gas usually had a considerable negative influence on the activity of traditional VWTi or VMoTi catalyst and it had been proved that SO₂ would affect the alkali resistance of catalysts [18]. The fresh CuNbTi catalyst has been proved to exhibit an excellent sulfur resistance in our previous report [12]. Hence, the impact of SO₂ on 2% K₂O-CuNbTi at 325 °C was investigated in this work and the corresponding results were presented in Fig. 2(b). The NH₃-SCR reaction over 2%K₂O-CuNbTi catalyst was kept stable for 1 h before SO₂ was added. The NO_x conversion and N₂ selectivity kept 74% and 98%, respectively. When 50 ppm SO₂ was fed into the stream, NO_x conversion decreased to 68% firstly and then increased to 76%. After that, 250 ppm SO₂ was added and the NO_x conversion continued increasing to 79%. Meanwhile, the N₂ selectivity maintained above 97% within the entire reaction process. These results indicated that SO₂ improved the NO_x conversion, which could be attributed to the enhanced surface acidity [19] and SO₂ did not pose the negative effect on the activity of 2%K₂O-CuNbTi catalyst.

Fig. 2(c) showed the NO_x conversion and N₂ selectivity of 2%K₂O-CuNbTi catalyst under the coexistence of H₂O and SO₂ at the reaction temperature of 325 °C. It was obvious that the coexistence of 5%H₂O and 250 ppm SO₂ induced a decrease of the catalytic activity that the NO_x conversion dropped from 74% to 64% while the N₂ selectivity decreased from 98% to 94%. It was commonly accepted that the loss of NH₃-SCR activity was closely relevant with the formation and deposition of ammonium sulfate on the surface of catalyst during H₂O and SO₂ coexisting in the feed stream [20,21]. After 5%H₂O and 250 ppm SO₂ were cut off, the catalytic activity recovered gradually to some extent that NO_x conversion kept about 69% and N₂ selectivity maintained 97%, which was lower than the initial value, suggesting the coexistence of H₂O and SO₂ had an inhabitation effect on the 2%K₂O-CuNbTi catalyst.

3.2. Physicochemical properties

3.2.1. Morphological analysis

The representative SEM patterns of fresh and poisoned CuNbTi and VWTi catalysts were obtained to investigate the morphology change, as shown in Fig. 3S. It was remarkable that particle agglomerated after potassium loading on CuNbTi and VWTi catalysts. Compared with fresh catalysts, the potassium additive resulted in the active phase agglomeration over the surface of catalysts, which had a negative effect on the NH₃-SCR activity [1]. Furthermore, the extent of agglomeration over 2%K₂O-VWTi was severer than 2K₂O-CuNbTi. This might be related with that 2%K₂O-VWTi catalyst was almost completely deactivated while 2K₂O-CuNbTi catalyst still exhibited 80% NO_x conversion.

3.2.2. Textural characteristics

The microstructure characteristics of fresh and K₂O-poisoned catalysts were firstly analyzed by using XRD patterns and the results were shown in Fig. 4S. All of the four samples mainly represented the anatase phase. Some rutile phase existed in VWTi and 2%K₂O-VWTi catalysts, which was related to the support P25 TiO₂ containing 15% rutile TiO₂ phase. CuNbTi and 2%K₂O-CuNbTi were well indexed to anatase TiO₂ (PDF-ICDD 99-0008) while VWTi and 2%K₂O-VWTi were well indexed to anatase TiO₂ (PDF-ICDD 86–1157). Furthermore, the diffraction peaks of CuNbTi catalysts were broader and the peak intensities were weaker than those of VWTi catalysts, which was attributed to the function of Nb₂O₅ on TiO₂ in the CuNbTi system [12]. Slight changes were observed and this proved that K₂O doping did not alter the crystalline structure of CuNbTi and VWTi catalysts. In addition, the crystal particle sizes were calculated using Scherrer equation, as shown in Table 1. The grain sizes of CuNbTi and VWTi decreased from 9.3 nm and 27.4 nm to 9.0 nm and 26.3 nm, respectively. The smaller crystallite of K₂O-poisoned catalysts indicated that loading of potassium oxides inhibited the grain growing, resulting in a drop of NO_x conversion [5].

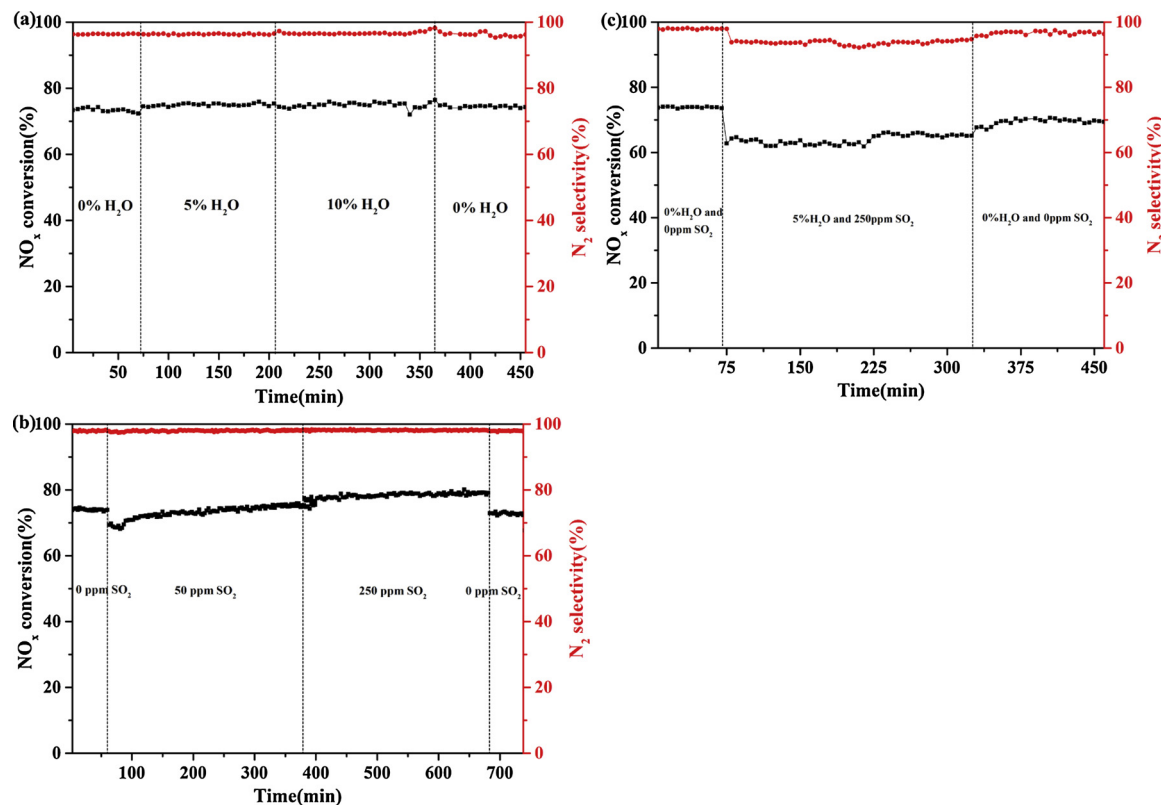


Fig. 2. Effect of (a) H_2O , (b) SO_2 , (c) H_2O and SO_2 on the NH_3 -SCR activity of 2% K_2O -CuNbTi catalyst at 325 °C. Reaction conditions: $[\text{NH}_3] = [\text{NO}_x] = 500 \text{ ppm}$, $[\text{H}_2\text{O}] = 5\text{--}10\%$ (when used), $[\text{SO}_2] = 50\text{--}250 \text{ ppm}$ (when used), $[\text{O}_2] = 5\%$, total flow rate = 500 mL min^{-1} , GHSV = 177,000 h^{-1} and N_2 as balance.

The Brunauer-Emmett-Teller (BET) surface areas, total pore volume and average pore diameter of various catalysts were summarized in Table 1. The surface areas of CuNbTi and VWTi catalysts were 73.1 m^2/g and 46.0 m^2/g respectively while those of the K_2O -doped catalysts declined to 69.3 m^2/g and 32.1 m^2/g , respectively. This indicated that K_2O had a blocking or depositing effect on the sample [19]. Also, both the pore volume and diameter reduced obviously with K_2O loading on VWTi catalysts. This might explain the deactivating effect of K_2O loading on VWTi catalysts [8]. On the contrary, the K_2O poisoned CuNbTi catalyst showed a higher total pore volume (0.32 cm^3/g) and average pore diameter (16.9 nm) than the fresh CuNbTi catalyst (0.29 cm^3/g and 11.5 nm). Hence, the preservation of total pore volume and average pore diameter on 2% K_2O -CuNbTi catalyst would be in favor of maintaining active sites for NH_3 -SCR reaction. This supported the conclusion that 2% K_2O -CuNbTi catalyst kept a well activity while 2% K_2O -VWTi deactivated completely.

The surface atom environment of the samples was investigated by XPS and the results were displayed in Fig. 3. Ti 2p, Nb 3d, Cu 2p and O 1s were analyzed and the main surface metal content was summarized in Table 2.

Fig. 3(a) displayed the spectra of Ti 2p with two binding energy of Ti 2p_{1/2} and Ti 2p_{3/2}. For CuNbTi and 2% K_2O -CuNbTi, the peaks of Ti 2p_{1/2} were located at 464.70 eV while the peaks of Ti 2p_{3/2} were at 458.97 eV, which were the characteristics of Ti^{4+} species in anatase

TiO_2 [21]. The binding energy kept nearly unchanged for the fresh and 2% K_2O poisoned CuNbTi catalyst, illustrating that potassium had little influences on titanium of Ti_2NbO_x support.

The Nb 3d XPS spectra of CuNbTi and 2% K_2O -CuNbTi were presented in Fig. 3(b), which were consisted of Nb 3d_{3/2} and Nb 3d_{5/2}. The peaks of Nb 2p_{3/2} were located at 210.60 eV and 209.32 eV while the peaks of Nb 2p_{1/2} were at 207.90 eV and 206.65 eV over CuNbTi and 2% K_2O -CuNbTi catalyst, respectively. All of them were the characteristic peaks of Nb^{5+} species [22]. However, the existential status of Nb^{5+} species over CuNbTi catalyst was mainly Nb_2O_5 [23] while Nb^{5+} existing in KNbO_3 compound on the 2% K_2O -CuNbTi catalyst [23,24]. It was obvious that the peaks of Nb 3d shifted to a lower binding energy after 2% K_2O poisoned. The binding energy would change (shifted to a lower direction or a higher direction) when the density and arrangement of electron cloud transformed according to some literatures [25,26]. An increasing of electron cloud density would result in the binding energy shifting to a lower direction while the decreasing of electron cloud density was related to a higher direction offset [25]. And the formation of KNbO_3 according to XPS results confirmed that $\text{Nb}=\text{O}$ and $\text{Nb}-\text{OH}$ were transformed to $\text{Nb}-\text{O}-\text{K}$, which enhanced the electron cloud arrangement of niobium atom and shifted the peaks to a lower binding energy direction. As a result, there was a fairly strong interaction between K and niobium species and K was trapped by Ti_2NbO_x support.

Table 1

BET surface area and pore parameters of catalysts measured by N_2 adsorption experiments and particle size calculated by Scherrer equation from XRD experiments.

Samples	Surface area(m^2/g)	Total pore volume(cm^3/g)	Average pore diameter(nm)	Lattice parameter(Å)	Crystallite (nm)
CuNbTi	73.1	0.29	11.5	3.808	9.3
2% K_2O -CuNbTi	69.3	0.32	16.9	3.796	9.0
VWTi	46.0	0.40	32.7	4.7091	27.4
2% K_2O -VWTi	32.1	0.24	28.0	4.509	26.3

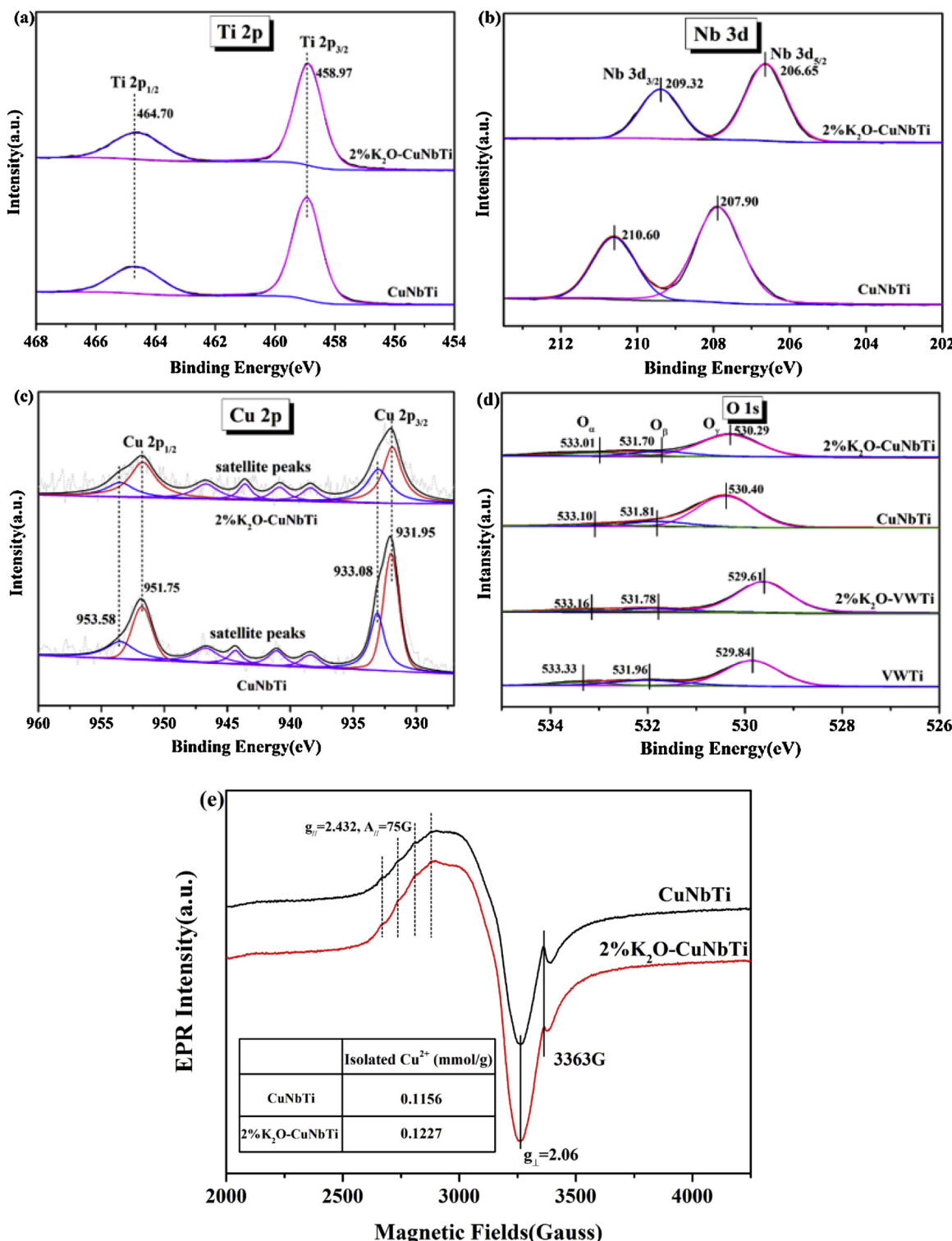


Fig. 3. The surface atom status and environment of fresh and 2%K₂O poisoned catalysts: XPS spectra of (a) Ti 2p, (b) Nb 3d, (c) Cu 2p, (d) O 1s; And (e) EPR spectra of CuNbTi and 2%K₂O-CuNbTi.

Copper species as active components were also scanned and the Cu 2p spectrum was shown in Fig. 3(c). There were mainly Cu 2p_{1/2} and Cu 2p_{3/2} corresponding to different kinds of copper and some satellite peaks existing between 935 eV and 950 eV, which were considered as bivalent copper species [21]. The Cu 2p_{3/2} was fitted into two peaks at 931.95 eV and 933.08 eV, referred to Cu⁺ species and Cu²⁺, respectively [27]. And the Cu 2p_{1/2} was also split into two peaks located in 951.75 eV and 953.58 eV, which were ascribed to Cu⁺ and Cu²⁺,

respectively [21]. Hence, the copper species mainly existed with two valence states over CuNbTi and 2%K₂O-CuNbTi catalysts. It was widely accepted that the redox cycle between Cu²⁺ and Cu⁺ species played an important role in the activity of NH₃-SCR over copper-based catalysts, and the appearance of Cu⁺ species was proved to be related to the NO_x reduction activity [28]. So, the relative content of Cu⁺/(Cu²⁺ + Cu⁺) was calculated, as shown in Table 2. The Cu⁺ species decreased (Cu²⁺ increased) slightly after K₂O was added, demonstrating that K₂O had an

Table 2
Main surface metal content of different samples.

samples	Atom concentration (%)						Atom ratio (%)	
	Ti	Nb	O	Cu	W	V	$(O_\alpha + O_\beta)$ ratio	Cu^+ ratio
CuNbTi	18.73	10.84	69.05	1.37	–	–	25.85	48.03
2%K ₂ O-CuNbTi	18.61	11.20	69.35	0.84	–	–	26.46	46.59
VWTi	29.29	–	65.24	–	3.55	1.92	28.12	–
2%K ₂ O-VWTi	29.80	–	65.25	–	3.56	1.39	19.05	–

effect on the redox of Cu^{2+} and Cu^+ .

NH_3 -SCR was a reaction with participation of oxygen and the surface active oxygen species were crucial to catalytic activity [29]. Hence, O 1 s over the surface of catalyst was investigated and the results were shown in Fig. 3(d). The spectra demonstrated asymmetric peaks, which could be fitted into three bands with a primary band (O_γ) and two sub-bands (O_α and O_β). Generally, the bands (O_γ) at 529.61–530.40 eV corresponded to the lattice oxygen O^{2-} [30–32]. And the ones (O_β) at 531.70–531.96 eV could be assigned to surface chemisorbed oxygen species or ionization of oxygen species, such as OH^- , O_2^{2-} , O^- and CO_3^{2-} [19,33]. Another sub-bands (O_α) at 533.01–533.33 eV were considered as the hydroxyl species (OH^-) or adsorbed water [19,34]. Both of O_α and O_β belonged to surface active oxygen species due to their higher mobility, which were favored to the oxidation of NO to NO_2 and the redox circulation between active species of different valence states [19]. All of these impacts would facilitate to the process of NH_3 -SCR reaction. And then the relative ratio of $(O_\alpha + O_\beta) / (O_\alpha + O_\beta + O_\gamma)$ was quantified according to the O 1 s spectra, as shown in Table 2. The ratio of surface active oxygen over 2%K₂O-VWTi was 19.05%, lower than that of VWTi (28.12%), revealing the restraining effects of K₂O on the labile oxygen species in VWTi catalyst. Interestingly, 2%K₂O-CuNbTi catalyst had a higher ratio (26.46%) than the fresh one (25.85%). The increase of labile oxygen over 2%K₂O-CuNbTi contributed to maintain the catalytic performance of 2%K₂O-CuNbTi catalyst. Compared with fresh CuNbTi and VWTi catalyst, the binding energy of O 1 s shifted to a lower direction for K₂O poisoned catalyst, which was explained by the formation of chemical bonds between metal-dopant and active oxygen centers [35]. The poisoning element K increased the electron density among the valence shell of O atom. Some previous researches indicated that K could coordinate with both the vanadium and tungsten species, especially for the $V=O$, $V-OH$, $W=O$ and $W-OH$ on VWTi catalyst, forming $V-O-K$ and $W-O-K$ [8,36]. Meanwhile, K mainly interacted with $Nb=O$ and $Nb-OH$ and formed $Nb-O-K$ over CuNbTi system. All of them would lead to an increase of

electron cloud density of O atom and an excursion towards lower direction for O 1 s peaks.

To further investigate the transformation of copper species, EPR analysis was applied to characterize isolated Cu^{2+} , which was the only one to have EPR signals among all of the existence forms of copper species [37]. Isolated Cu^{2+} has been proved to be the main active specie over CuNbTi catalyst in our previous researches. Fig. 3(e) presented the EPR profiles of fresh and 2%K₂O poisoned CuNbTi catalysts. Both of them showed similar hyperfine structure with $g_{//} = 2.432$, $A_{//} = 75$ G and $g_{\perp} = 2.06$, which represented the isolated Cu^{2+} in anatase matrix [12]. Also, the peaks of 3363 G represented the support Ti_2NbO_x and it became weakened after K₂O loading, indicating that K₂O had an influence on the support, which was in accordance with the XPS results. Then the isolated Cu^{2+} was quantified and the results were inserted in Fig. 3(e). 2%K₂O-CuNbTi had a higher content of isolated Cu^{2+} (0.1227 mmol/g) than CuNbTi (0.1156 mmol/g). The increment of isolated Cu^{2+} after K₂O loading was in agreement with the results of XPS. Therefore, the data of XPS and EPR indicated that K₂O had an influence on Ti_2NbO_x , but the increasing content of isolated bivalent copper species maintained the NH_3 -SCR activity to some degrees over 2%K₂O-CuNbTi catalyst.

3.2.3. Surface acidity

Surface acidity of fresh and K₂O poisoned CuNbTi and VWTi catalysts were investigated using NH_3 -TPD methods and the curves were shown in Fig. 4(a). Meanwhile, in situ DRIFTS were performed to investigate the types of acid sites at different temperatures (Fig. 5). CuNbTi showed two peaks at 278 °C and 340 °C while 2%K₂O-CuNbTi established two desorption peak at 204 °C and 283 °C. As for VWTi catalyst, three desorption peaks centered at 233 °C, 341 °C and 458 °C were detected, indicating abundant acid sites over VWTi catalyst. However, there was nearly no desorption peak for 2%K₂O-VWTi catalyst. According to previous researches, the peaks below 300 °C were considered as the weakly chemisorbed NH_3 (weak and moderate acid sites) and the peaks under higher desorption temperature were regarded as the strongly chemisorbed NH_3 , namely strong acid sites [38]. Compared with fresh CuNbTi and VWTi catalysts, the total acid sites of 2%K₂O poisoned samples declined apparently. 2%K₂O-CuNbTi preserved the weak acid sites while 2%K₂O-VWTi lost almost all of its acidity, which certified the favorable alkali resistance for CuNbTi catalyst.

Fig. 5 illustrated the results of in situ DRIFTS spectra of NH_3 -TPD over CuNbTi, 2%K₂O-CuNbTi, VWTi and 2%K₂O-VWTi catalysts. The negative bands at about 3679 cm⁻¹ for CuNbTi catalyst were assigned to the hydroxyl groups (Nb-OH) consumed during the process of NH_3 chemisorbing on the surface of catalyst to form NH_4^+ [30]. And the

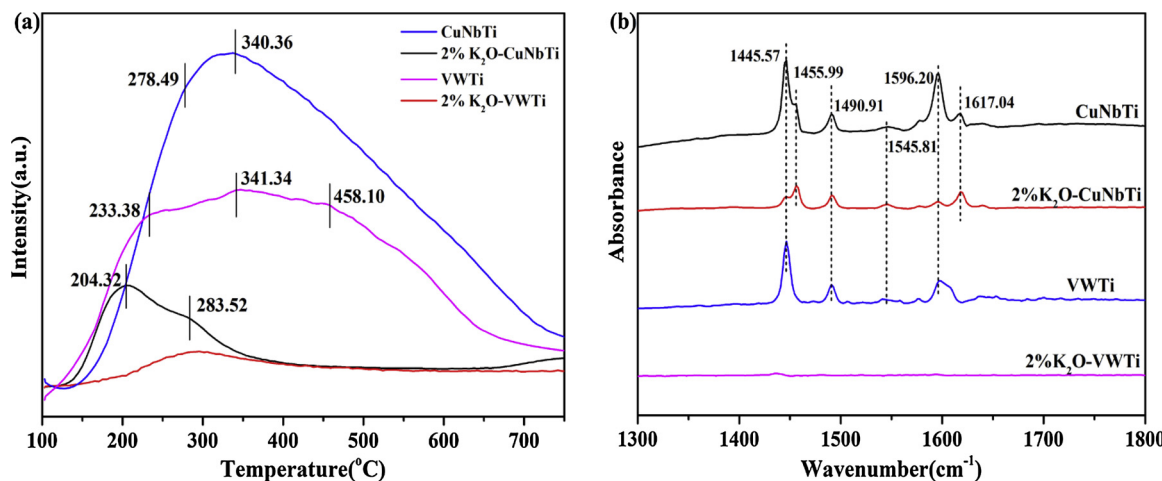


Fig. 4. (a) NH_3 -TPD and (b) Pyridine-IR profiles of fresh and K₂O poisoned catalysts.

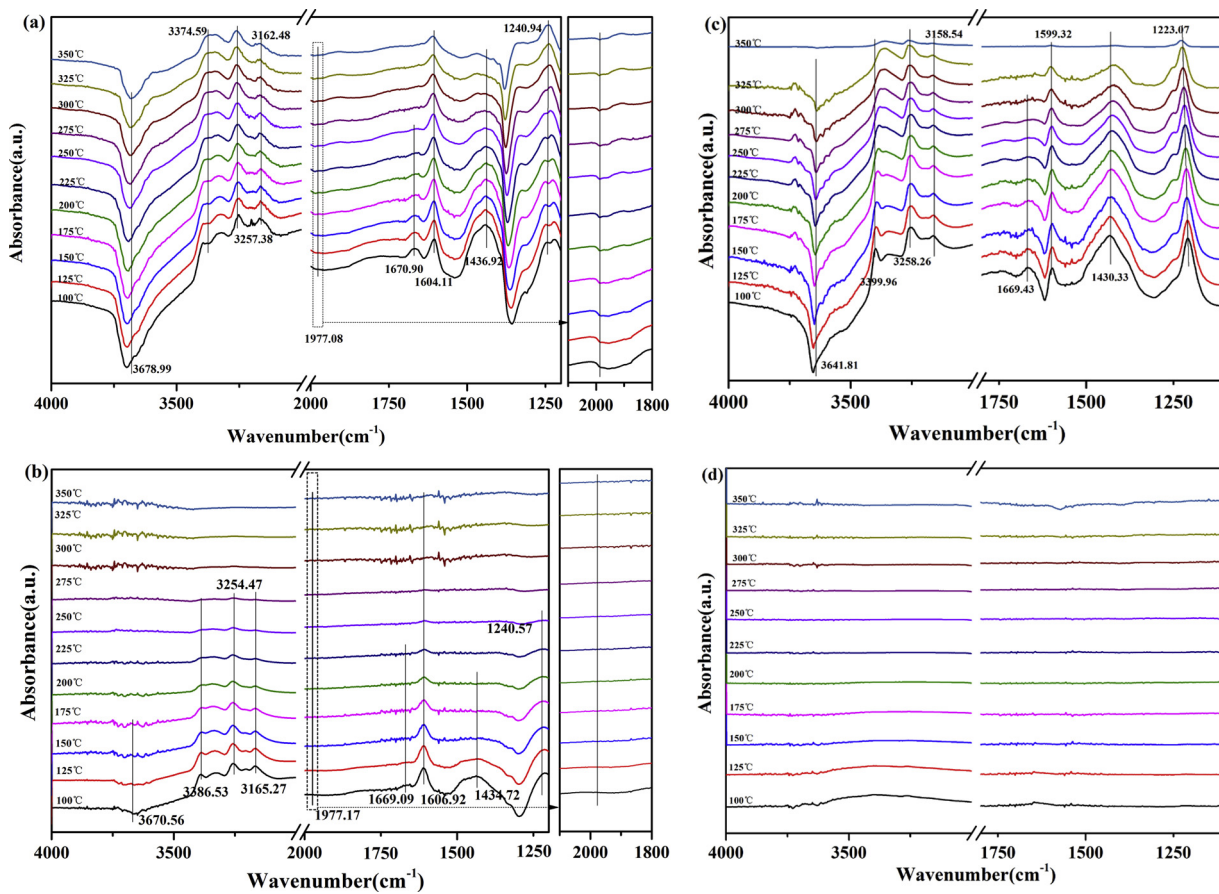


Fig. 5. in situ DRIFTS spectra of NH_3 adsorption in 1000 ppm NH_3/N_2 at 100 °C for 1 h and then purged with N_2 before temperature programmed from 100 to 350 °C over (a) CuNbTi, (b) 2%K₂O-CuNbTi (c) VWTi and (d) 2%K₂O-VWTi catalysts.

$\text{Nb}=\text{O}$ corresponding to the band at 1977 cm^{-1} was also consumed during the NH_3 adsorption [30]. Nevertheless, the bands representing $\text{Nb}-\text{OH}$ became weakly at 100 °C and $\text{Nb}=\text{O}$ vanished over 2%K₂O-CuNbTi catalyst. This result declared that the presence of K₂O consumed $\text{Nb}=\text{O}$ and $\text{Nb}-\text{OH}$ over CuNbTi, leading to a decrease of surface acid sites. Also, the negative band at 3642 cm^{-1} for VWTi belonged to the consumption of V-OH [39]. Three bands at about 3375–3399 cm^{-1} , 3254–3258 cm^{-1} and 3158–3165 cm^{-1} observed on CuNbTi, 2%K₂O-CuNbTi and VWTi catalysts were attributed to the N–H stretching vibration modes coordinated NH_3 [5,39]. The bands centered at approximately 1600–1607 cm^{-1} and 1223–1241 cm^{-1} could be ascribed to bending vibrations of N–H bonds in NH_3 coordinately linked to Lewis acid sites [6,8,40], while the other peaks at 1669–1771 cm^{-1} and 1430–1437 cm^{-1} were assigned to bending vibrations of ionic NH_4^+ on the Brønsted acid sites [32,41]. As for CuNbTi catalyst, the intensity of the bands at 1669–1771 cm^{-1} and 1430–1437 cm^{-1} reduced noticeably with the increase of temperature. On the contrary, the intensity of bands at 1223–1241 cm^{-1} decreased slightly and the bands at 1600–1607 cm^{-1} remained the same with the temperature rising from 100 °C to 350 °C. Hence, Lewis acid sites presented a better thermal stability than Brønsted acid sites. After doping 2%K₂O, the bands corresponding to the NH_4^+ on the Brønsted acid sites disappeared at 150 °C and the bands representing the N–H bonds coordinately linked to Lewis acid sites vanished gradually at 250 °C, suggesting that the presence of K₂O decreased the amount of acid sites and weakened the strength of acidity over CuNbTi. When compared to VWTi catalyst (as shown in Fig. 5(c)), all of the bands relating to Lewis and Brønsted acid sites declined gradually with the temperature increasing from 100 °C to 350 °C, showing a weaker acidity than CuNbTi catalyst. But 2%K₂O loading resulted in the total loss of acid sites on

VWTi as no NH_3 adsorption bands were existed in Fig. 5(d). According to the results of in situ DRIFTS, the peaks below 300 °C could be identified as NH_3 desorption from most of Brønsted acid sites and some Lewis acid sites while the peaks higher 300 °C were caused by NH_3 adsorption on Lewis acid sites. NH_3 adsorption-desorption experiments proved that some acid sites were reserved for the 2%K₂O-CuNbTi catalyst while no acid sites available for NH_3 absorption over 2%K₂O-VWTi catalyst.

The Pyridine-IR spectra of fresh and K₂O poisoned catalysts were shown in Fig. 4(b). CuNbTi and 2%K₂O-CuNbTi showed similar bands. The bands at 1445 cm^{-1} and 1596 cm^{-1} on both CuNbTi and VWTi catalysts were ascribed to the Lewis acid sites while the bands of 1456 cm^{-1} and 1617 cm^{-1} only existing over the CuNbTi catalyst were also thought to be the Lewis acid sites [17]. And the rest bands at 1491 cm^{-1} and 1546 cm^{-1} for CuNbTi and VWTi catalysts were attributed to Brønsted acid sites [42]. The quantities of different acid sites were calculated and shown in Table 3. So, it could be concluded from the results of Pyridine-IR experiments that Lewis acid sites were the dominant acid sites over CuNbTi and VWTi catalyst. However, the total

Table 3
The quantities of different acid sites over fresh and K₂O poisoning catalysts.

	Brønsted acid sites($\mu\text{mol/g}$)	Lewis acid sites($\mu\text{mol/g}$)	Total acid sites($\mu\text{mol/g}$)	Brønsted/Lewis
CuNbTi	44.94	446.80	491.74	0.10
2%K ₂ O-CuNbTi	24.56	143.75	168.31	0.17
VWTi	10.78	284.14	294.92	0.04
2%K ₂ O-VWTi	3.08	3.43	6.51	0.90

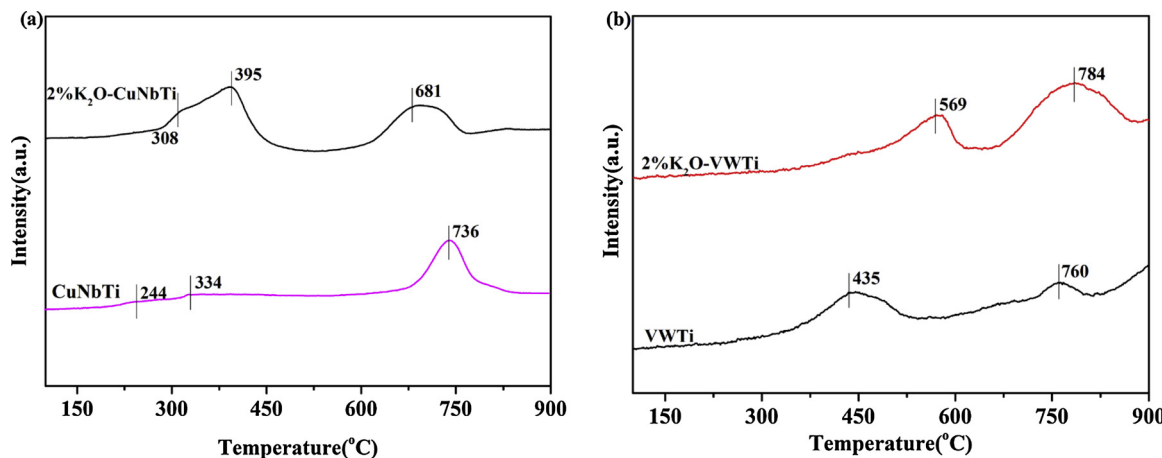


Fig. 6. H_2 -TPR profiles of fresh and 2% K_2O poisoned (a) CuNbTi and (b) VWTi catalysts.

acid sites on CuNbTi decreased from 491.74 $\mu\text{mol/g}$ to 168.31 $\mu\text{mol/g}$ after K_2O doping while it reduced from 294.92 $\mu\text{mol/g}$ to 6.51 $\mu\text{mol/g}$ after K_2O deactivated the VWTi catalyst. Obviously, 2% K_2O -CuNbTi kept some acid sites although both of Lewis acid sites and Brønsted acid sites brought down to some extent, but 2% K_2O -VWTi lost nearly all of its acid sites, which was in accordance with the results of NH_3 -TPD and *in situ* DRIFTS. As a consequence, more acid sites on 2% K_2O -CuNbTi than 2% K_2O -VWTi contributed to its alkali-resistance.

3.2.4. Redox properties

H_2 -TPR was performed to characterize the redox properties of different catalysts and the results were reported in Fig. 6. In our previous studies, the isolated Cu^{2+} was reduced to Cu^+ at 244 °C and then Cu^+ was converted to copper metallic at 334 °C. The peaks at 736 °C were attributed to the reduction of Nb_2O_5 to Nb_2O_4 . For 2% K_2O -CuNbTi (Fig. 6(a)), the reduction peak of Cu^{2+} to Cu^+ and Cu^+ to copper metallic shifted to 308 °C and 395 °C, respectively. The reduction temperature of copper increased after K_2O doping on CuNbTi catalyst, which suggested a drop in the reducibility of bivalent copper ions over 2% K_2O -CuNbTi catalyst, resulting in a decrease of catalytic performance. As for the reduction temperature, both of physical texture and chemical property of catalyst would have an influence on the reducibility of active component. Delimaris [43] has proposed that the agglomeration of $\text{Cu}_x\text{Ce}_{1-x}$ catalyst led the low-temperature reduction peak of copper shifted to higher temperatures. The reduction peaks of V^{5+} to V^{3+} and W^{6+} to W^{4+} was proved to shift towards a higher temperature due to the coverage of alkali oxides over the surface of VWTi catalyst and the aggregation of bulk catalyst after alkali deactivating VWTi catalyst [44]. It was remarkable that particle agglomerated after potassium loading on CuNbTi catalyst according to SEM patterns and the surface area of 2% K_2O -CuNbTi catalyst declined from 73.1 m^2/g to 69.3 m^2/g from N_2 -physisorption experiment. These changes of physical texture might promote the reduction temperature of Cu^{2+} to Cu^+ rising. On the other hand, the reduction temperature would also be affected by the chemical properties of catalyst [45,46]. The formation of CaWO_4 could disrupt the interaction of V_{x}O_y and WO_x then lessen the reducibility of V^{5+} and W^{6+} species, leading to a higher reduction temperature over Ca-poisoned VWTi catalyst [8]. Also, Chen [36] attributed the increase of reduction temperature to the influence of Na and/or K on the chemical environment around V and W species over alkali-doped VWTi catalyst. As for 2% K_2O -CuNbTi catalytic system, Bader Charge analysis was then conducted to further investigate the rise of reduction temperature for bivalent Cu over CuNbTi and 2% K_2O -CuNbTi catalysts. And the results indicated that the charge distribution of copper over CuNbTi catalyst was 0.77 while it was 0.70 for 2% K_2O -CuNbTi catalyst. After K_2O doping, the charge distribution of copper decreased from 0.77 to 0.70, indicating that the reducibility of copper

was weakened. This might explain the reduction temperature of Cu^{2+} to Cu^+ shifting from 244 °C to 308 °C. In the meantime, the introduction of potassium and the transformation of KNbO_3 produced an effect on the chemical environment of Cu^{2+} over 2% K_2O -CuNbTi catalyst, which was another reason for the reduction temperature of Cu^{2+} to Cu^+ rising.

The reduction peak of Nb_2O_5 became broader and shifted to lower temperature from 736 °C to 681 °C, indicating that K_2O doping led to reduction of Nb_2O_5 more easily. Additionally, it is commonly considered that the peak area or intensity reflected the consumption of hydrogen. And it was apparent that H_2 consumption of Cu^{2+} for 2% K_2O -CuNbTi was much more than that for CuNbTi, indicating more Cu^{2+} existing over 2% K_2O -CuNbTi catalyst, which was consistent with the results of XPS and EPR. More Cu^{2+} resulted in more H_2 consumption during the temperature programmed reduction of hydrogen.

There were two reduction peaks over VWTi and 2% K_2O -VWTi catalysts, as shown in Fig. 6(b). The first reduction peak at 435 °C on VWTi catalyst could be assigned to the reduction of V^{5+} to V^{3+} and W^{6+} to W^{4+} [4] while the high temperature peak at 760 °C belonged to the reduction of W^{4+} to W^0 [47]. Obviously, two peaks shifted to 569 °C and 784 °C after deactivation, respectively. So, 2% K_2O severely suppressed the reducibility of active vanadia and tungsten oxide species. The H_2 consumption decreased at 569 °C while the reduction peak for W^{4+} became larger, which was coincide with the results of previous researchers [29]. Thus, we could conclude that K_2O weakened the reducibility of vanadium species and damaged the interaction of vanadium species and tungsten species, which was essential for NH_3 -SCR reaction [48].

3.3. Reaction mechanism

The synergistic promotional effect between copper species and niobium species over CuNbTi was proved to play a significant role in the catalytic activity in our previous investigations [12]. To further explore the synergistic mechanism in alkali resistance, 2% K_2O -NbTi and 2% K_2O -CuTi catalysts were also synthesized and the catalytic activity measurements were performed without 5% H_2O existing in the simulating mixture gas. As shown in Fig. 2S, 2% K_2O -NbTi deactivated among the whole range of reaction temperature, with less than 10.4% NO_x conversion and a maximum N_2 selectivity of 85.3%. 2% K_2O -CuTi exhibited a better activity than 2% K_2O -NbTi, but the NO_x conversion only achieved 10%–23% in the temperature range of 300–425 °C. Whereas 2% K_2O -CuNbTi showed the best activity since its maximum NO_x conversion was 73.8% while N_2 selectivity remained above 85% in the whole temperature range. N_2 selectivity of three catalysts was in the following sequence: 2% K_2O -CuNbTi > 2% K_2O -CuTi > 2% K_2O -NbTi. Therefore, the synergistic promotional effect also existed in the process

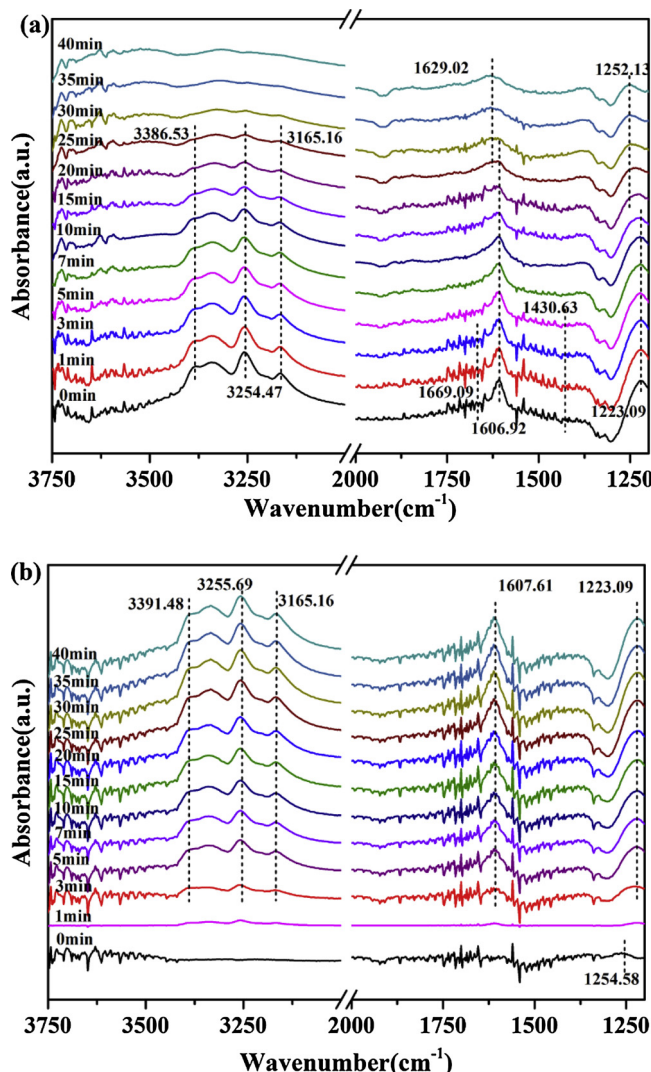


Fig. 7. in situ DRIFTS spectra of (a) gaseous NO and O₂ reacted with pre-adsorbed NH₃ species and (b) gaseous NH₃ and O₂ reacted with pre-adsorbed NO + O₂ species at 225 °C over 2%K₂O-CuNbTi. Reaction conditions: [NH₃] = 1000 ppm (when used), [NO] = 1000 ppm (when used), [O₂] = 5%, total flow rate = 100 mL min⁻¹ and N₂ as balance.

of alkali resistance. The experiments' results in section 3.2 indicated that Ti₂NbO_x could trap K₂O, protecting the active species of isolated Cu²⁺ and that copper species preserved a certain amount of acid sites and active species over the surface of 2%K₂O-CuNbTi catalyst for the NH₃-SCR reaction.

Temperature programmed surface reaction was conducted using in situ DRIFTS at 225 °C to learn about the reaction mechanism. Firstly, the catalyst was exposed in 1000 ppm NH₃/N₂ (100 ml/min) for 1 h to be saturated and then purged with N₂ (100 ml/min) for 30 min to eliminate physisorption NH₃. After that, 1000 ppm NO/N₂ and 5% O₂ was introduced and the spectra were recorded as a function of time. As shown in Fig. 7(a), several bands at 3386 cm⁻¹, 3254 cm⁻¹, 3165 cm⁻¹ attributed to the N–H stretching vibration modes coordinated NH₃ and other bands at 1607 cm⁻¹, 1223 cm⁻¹ assigned to the bending vibrations of N–H bonds in NH₃ coordinately on Lewis acid sites were detected after pre-adsorbed NH₃ following by N₂ purging. However, NH₄⁺ on the Brønsted acid sites at the bands of 1670 cm⁻¹ and 1431 cm⁻¹ were not observed due to the weak stability at 225 °C, which could be verified by in situ DRIFTS of NH₃-TPD. The surface NH₃ species were expended gradually after NO and O₂ introduction. At the same time, some new bands at 1629 cm⁻¹ and 1252 cm⁻¹ were

appeared at 25 min. For the band at 1629 cm⁻¹, some researchers regarded the band at 1620 cm⁻¹ as the bridging nitrates [19,49] while others attributed it to the δ_{HOH} vibration [8,50]. Combined with Fig. 7(b), the bands at 1620 cm⁻¹ did not arise after NO and O₂ adsorption with N₂ purging. So the band at 1620 cm⁻¹ in this study was ascribed to δ_{HOH} vibration, confirming the formation of H₂O. The band at 1252 cm⁻¹ was attributed to bidentate nitrate [5]. The reaction of NO and O₂ with pre-adsorbed NH₃ indicated that the reaction followed Eley-Rideal (E-R) mechanism over 2%K₂O-CuNbTi at 225 °C. However, it was really different that only one nitrate (bidentate nitrate) generated over 2%K₂O-CuNbTi catalyst while both monodentate nitrate and bridging nitrate emerged for CuNbTi catalyst, which was proved in previous research [12].

The reactivity of gaseous NH₃ and O₂ with pre-adsorbed NO + O₂ was also performed. After the activation under 350 °C for 30 min, the sample was cooled down to 225 °C. Then 1000 ppm NO (N₂ as balance) and 5% O₂ (by volume) were fed into the reactor for 1 h until adsorption saturation. Afterwards, the catalyst was purged with N₂ (1000 ml/min) for 30 min and then 1000 ppm NH₃ (N₂ as balance) with 5% O₂ (by volume) was introduced. The infrared spectra were collected at different time, as shown in Fig. 7(b). Only one band at 1255 cm⁻¹ (bidentate nitrate) was observed after NO and O₂ adsorption. The bidentate nitrate was consumed after 1 min and the NH₃ adsorbed species emerged at 3391 cm⁻¹, 3256 cm⁻¹, 3165 cm⁻¹, 1608 cm⁻¹ and 1223 cm⁻¹, indicating that the reaction over 2%K₂O-CuNbTi followed Langmuir-Hinshelwood (H-L) mechanism at 225 °C. Besides, it was obvious that Eley-Rideal mechanism played a dominant role in the reaction process.

3.4. Computational results

The geometric optimized structure of TiO₂ and Ti₂NbO_x was shown in Fig. 5S. In the model of Ti₂NbO_x, the ratio of titanium and niobium was 2/1 and niobium atoms replaced the sites of titanium atoms, which was consisted with our previous researching results [12]. Two different models of Ti₂NbO_x were selected as the main objects for the subsequence analysis (as shown in Fig. 5S(b)-(c)), which included all the possible adsorption sites for copper species. The valence state of Ti was +4 and Nb was +5 according to the Bader Charge analysis, which was consistent with the results of XPS in the previous work [12].

Then copper atoms were located on the surface of TiO₂ and Ti₂NbO_x, respectively. There were mainly two kinds of adsorption sites exposing, namely M=O and M–OH over the supports surface. Ti=O and Ti–OH were on the surface of TiO₂ while Ti=O, Ti–OH, Nb=O and Nb–OH existed over Ti₂NbO_x. All of the feasible supporting sites for Cu loading over Ti₂NbO_x were considered (as shown in Fig. 6S(a)-(b)) and the corresponding bonding energy (E_B) was examined (as depicted in Table 1S). Terminal Ti=O and Nb=O exhibited a higher activity among all sites for copper supporting. And the bridging coordination showed a more stable molecular geometry among all the coordinating modes. Fig. 6S(c)-(e) presented three bridging modes with different E_B. Obviously, the bonding energy of copper atom coordinating with two terminal oxygen atoms in O=Ti–O–Ti = O was -1.54 eV, which was the smallest value in all possible sites, indicating the most stable structure in this case. Meanwhile, the bonding energy of Nb=O–Cu–O–Nb (copper atom bonded with O=Nb–O–Nb=O) was -0.92 eV while it was -1.33 eV for Nb=O–Cu–O–Ti (copper atom coordinated with O=Nb–O–Ti = O), higher than that of Ti=O–Cu–O–Ti (copper atom coordinated with O=Ti–O–Ti=O). Compared with Nb=O, Ti=O exhibited a higher activity for copper linking to the surface of Ti₂NbO_x support. It was correlated with the ligancy of Ti⁴⁺, leading to unpaired electrons existing over the terminal Ti=O, which served as strong electron donor to bond with copper atom or hydrogen atom [17]. The bond length of Cu = O was in the range of 1.83 Å–1.86 Å.

To get insight into the alkali affinity for the CuNbTi catalyst, K atom

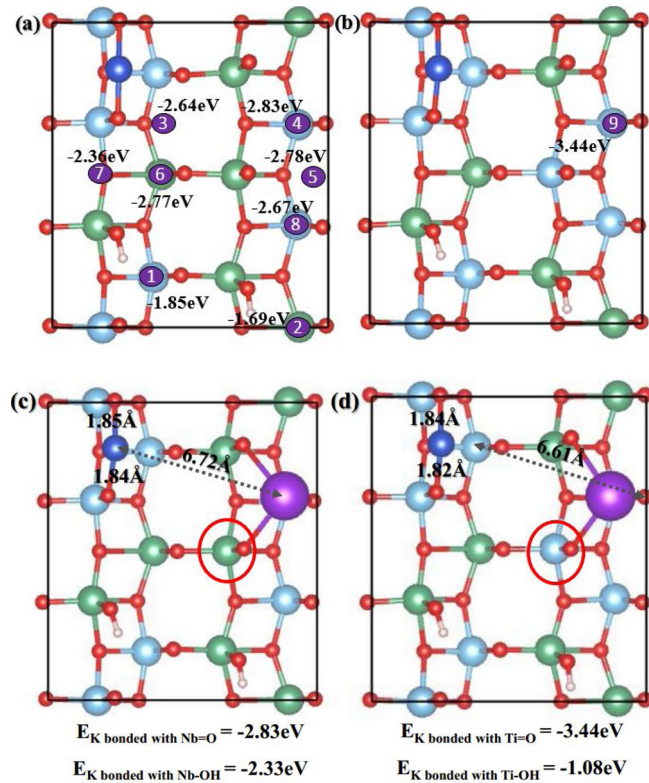


Fig. 8. (a)-(b) Possible sites for K locating at CuNbTi models and (c)-(d) the binding energy of K bonded with Nb=O, Nb-OH, Ti=O, and Ti-OH. ● represented Ti atom, ● represented Nb atom, ● represented Cu atom, ● represented H atom, ● represented O atom and ● represented the possible locating sites for K atoms.

was located on the surface of CuNbTi model. All the possible adsorption sites over the surface of Cu atom bonding with O=Ti–O–Ti=O in CuNbTi model were investigated and the bonding energy (E_{B-K}) was calculated in this computational experiment (Fig. 8(a)-(b)). The results of E_{B-K} suggested that K atom interacting with two Ti=O and one Nb=O simultaneously with -3.44 eV adsorption energy displayed the most stable status. Furthermore, the exposed local structures of Nb=O, Nb-OH, Ti=O, and Ti-OH would dramatically affect the interaction between K atom and CuNbTi catalyst.

In order to reveal the K poisoning and selectivity mechanism, K binding energy on those four function sites was calculated, as shown in Fig. 8(c)-(d). Two K-poisoning slab models and four different clean slab models were employed according to the definition of K binding energy. For eliminating other effects and simplifying the analysis process, the same structure models were constructed, in which there is only one different site being replaced by those four functional sites (marked with red circle) on the surface. So the binding energy was solely determined by four different functional sites. After calculating, the binding energy of K atom with four functional sites followed an order: Ti-OH (-1.08 eV) > Nb-OH (-2.33 eV) > Nb=O (-2.83 eV) > Ti=O (-3.44 eV). Nevertheless, Cu atom and H atom preferentially expended Ti=O on the basis of the process of CuNbTi catalyst being synthesized. Thus Nb=O and Nb-OH would interacted with K atoms over the CuNbTi catalyst. And the formation of KNbO₃ according to XPS results further confirmed the Nb=O and Nb-OH were transformed to Nb=O–K, which was consistent with this DFT calculation. Moreover, the bond length of Cu=O kept in the range of 1.82 Å–1.85 Å after K doping, indicating little effects of K on Cu. And the distance between Cu and K was 6.61 Å–6.72 Å.

Also, the structure of CuTi was built with the same method, as given in Fig. 7S. When CuTi catalyst was poisoned, the most stable structure

presented that K was close to Cu atom, interacting with bridging O, supporting O and terminal OH. The energy varied from -2.80 eV to -0.28 eV when K atom was close to and far from Cu atom, confirming the affinity of K for both copper unit and support phase with the former dominating. Compared with KCuNbTi catalyst, the distance between K atom and Cu atom over CuTi catalyst reduced from 6.72 Å to 4.14 Å. And the Cu=O distance of KCuTi was elongated from 1.78 Å to 1.80 Å–1.83 Å with respect to the CuTi. Hence, potassium doping showed a remarkable perturbation of Cu=O in CuTi catalyst while it nearly maintained the initial Cu=O for CuNbTi catalyst, manifesting the protective effect of the support on the active component from being poisoned by alkali over CuNbTi catalytic system. Copper species and niobium species exhibited the synergistic promotional effect towards anti-alkali, which was coincided with the experiments results in 3.3.

In order to investigate the surface acidity of catalyst, NH₃ was adsorbed on the fresh and K poisoned CuNbTi catalyst. The N atom in NH₃ molecular coordinating with Cu atom represented the Lewis acid sites while N atom connecting the external hydroxyl denoted the Brønsted acid sites [51,52]. Cu acted as the Lewis acid sites and both of Nb=O and Ti–OH served as the Brønsted acid sites for NH₃ adsorption. When NH₃ adsorbed on Cu of CuNbTi system, the effect of Nb=O around Cu was investigated, as shown in Fig. 9(a)-(c). The hydrogen of NH₃ molecular would interact with contrapuntal oxygen in this case. NH₃ molecular was adsorbed on Cu sites with two Nb=O around, exhibiting the most steady model with an adsorption energy of -1.10 eV. NH₃ could also adsorb on Nb=OH and Ti–OH with adsorption energy of -0.37 eV and -0.16 eV (shown in Fig. 9(d)–(e)), respectively. These results suggested that it was easier for NH₃ adsorbing on Lewis acid sites than Brønsted acid sites. After K doping (Fig. 9(f)–(g)), NH₃ adsorbed on Cu site with an adsorption energy of -0.62 eV and the bond length of H–O increased from 1.92 Å to 2.02 Å. This indicated that K doping could weaken the interaction between hydrogen of NH₃ molecular and contrapuntal oxygen in the catalyst, resulting in an increase of adsorption energy. Meanwhile, it was difficult for NH₃ adsorbing on Ti–OH as the E_{ads} was just -0.03 eV. The decrease of NH₃ adsorption sites and increase of adsorption energy was one of the reasons for the catalytic activity reducing over KCuNbTi catalyst.

Besides, the experiment of NH₃ adsorbing over KCuTi catalyst was also performed, as shown in Fig. 8S. The adsorption energy of NH₃ adsorbing on Cu in KCuTi system was -0.72 eV, higher than -1.10 eV of KCuNbTi, illustrating that K had a stronger inhibiting effect on CuTi catalyst. And the length of N–H bond for KCuTi was 1.71 Å–1.91 Å, larger than that of free NH₃ molecular (1.02 Å) [52] while it kept nearly unchanged for KCuNbTi (1.02 Å). The enlargement of N–H bond was related to the nonlocality of long pair electrons among the orbital of NH₃, which resulted in the migration of the electrons to Cu cation during the hybridization between NH₃ molecular and Cu atom [52,53]. Thus, compared with KCuTi, Ti₂NbO_x played an active role on NH₃ adsorption over KCuNbTi, weakening the effect of potassium on NH₃ adsorbing on the catalyst surface. To be concluded, potassium could be trapped by the Ti₂NbO_x support and the active copper species were protected over CuNbTi catalyst while potassium directly interacted with the copper on the CuTi catalyst and inhibited the activity of copper species and the adsorption of NH₃ molecular. These revealed a synergistic effect of copper and niobium in the process of anti-alkali poisoning over CuNbTi catalyst. All of these results verified the conclusions of the experiments.

For the VWTi catalyst, K atoms interacted with both the active V atoms and the support TiO₂ according to previous work and experimental results [4,54]. Therefore, alkali poisoning mechanisms were different for CuNbTi catalyst and VWTi catalyst. The active species of copper were protected in the CuNbTi catalyst while vanadium species were deactivated in the VWTi catalyst with potassium doping.

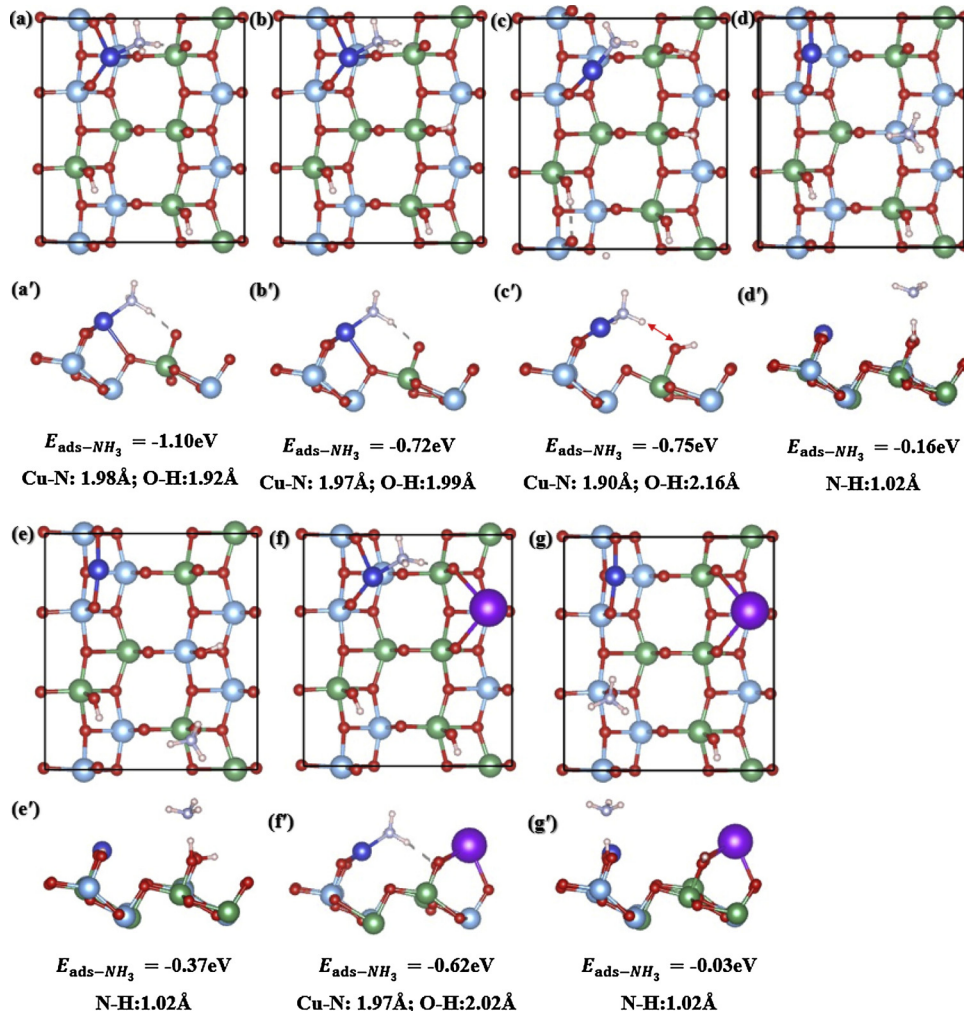


Fig. 9. NH_3 adsorbed on (a)-(e) (a')-(e') CuNbTi and (f)-(g) (f')-(g') KCuNbTi: (a)-(g) top view and (a')-(g') side view. (●) represented Ti atom, (●) represented Nb atom, (●) represented Cu atom, (●) represented K atom, (●) represented N atom, (●) represented H atom, and (●) represented O atom.

3.5. Discussions

All the results above demonstrated that CuNbTi catalyst exhibited greater alkali resistance than traditional VWTi catalyst. The poisoning mechanisms between CuNbTi and VWTi were really different, and the schematic models were shown in Fig. 10. A fundamental ion-exchange mechanism of VWTi deactivating by alkali was proposed that alkali metal ions reacted with protons from V-OH group, which was

Brønsted acid sites as the active phase for NH_3 -SCR reaction in previous researches [55,56]. Both of Brønsted acid sites (V-OH) and Lewis acid sites (V=O) reduced significantly from the results of NH_3 -TPD, Pyridine-IR and in situ DRIFTS in this work, which was the main reason for 2% K_2O -VWTi deactivation. The active vanadium species and support TiO_2 were poisoned in the 2% K_2O -VWTi system. Besides, it could be observed that there was agglomeration over the surface of VWTi catalyst and both of the surface area and the total pore volume decreased

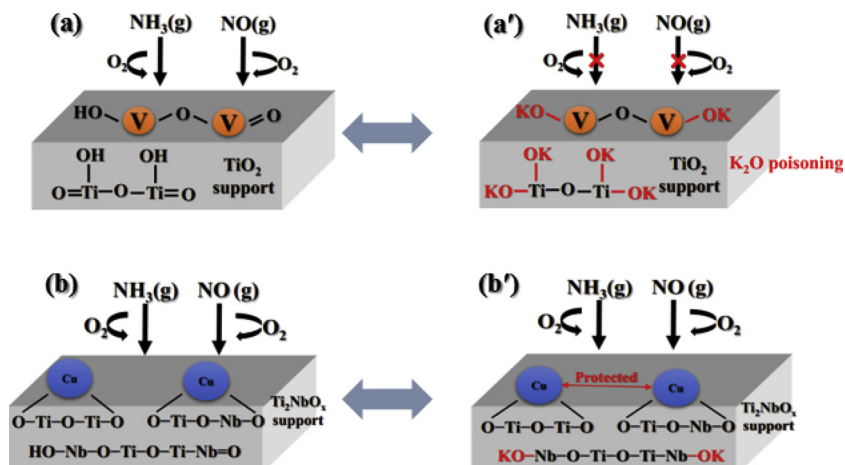


Fig. 10. Schematic model of 2% K_2O poisoning VWTi and CuNbTi catalysts: (a) fresh VWTi (a') 2% K_2O -VWTi (b) fresh CuNbTi (b') 2% K_2O -CuNbTi.

after K_2O doping. The surface active oxygen species over catalyst surface and the reducibility of 2% K_2O -VWTi reduced. It was certified that alkali would affect the dispersion of vanadium and tungsten species on the surface of support, resulting in the decrease of surface active oxygen and reducibility, which was also important factors of catalytic activity [8]. The transformation of physical structure and chemical properties for 2% K_2O -VWTi catalyst led to a deactivation. Nevertheless, the impact of K_2O on CuNbTi catalyst was really different. The pore volume increased while the surface area dropped. And K atoms were preferable to coordinate with Nb=OH and Nb=O of the Ti_2NbO_x support, indicating a strong interaction of K_2O with the support. This preserved enough surface chemisorbed active oxygen species and active isolated Cu^{2+} for NH_3 -SCR reaction, although some structural changes existed due to the presence of K_2O . Meanwhile, the interaction between K_2O and Ti_2NbO_x support prevented the destruction of active copper species by K_2O , and a certain amount of Brønsted acid sites and Lewis acid sites were reserved. And Ti_2NbO_x could also weaken the effect of potassium on NH_3 adsorption over KCuNbTi catalyst. Hence, 2% K_2O -CuNbTi catalyst could still remain 80% NO_x conversion efficiency. Niobium species and copper species were proved to present a synergistic role on the alkali resistance of CuNbTi catalyst. TiO_2 support with addition of niobium species trapped alkali K_2O while the isolated Cu^{2+} preserved remained the catalytic activity. And this work would provide a general strategy for developing novel anti-alkali poisoning NH_3 -SCR catalyst in the future.

4. Conclusions

In this work, CuNbTi catalyst exhibited a better alkali resistance than traditional commercial VWTi catalyst. 2% K_2O -CuNbTi achieved 80% NO_x conversion at 325 °C while 2% K_2O -VWTi was almost completely deactivated. K_2O doping resulted in agglomeration of CuNbTi and VWTi catalysts, hence decreasing the surface area. However, the channels and pores of VWTi were deposited and blocked by K_2O while the pores were preserved over CuNbTi catalyst, supplying active sites for the reaction. Meanwhile, K_2O was more liable to coordinate with Nb=OH and Nb=O with a lower bonding energy of $-2.33\text{ eV} - 2.83\text{ eV}$ over the CuNbTi catalytic system according to the results of experiments and DFT calculations. K_2O was trapped by Ti_2NbO_x support, forming $KNbO_3$ and protecting the active copper species from destruction to some extents. On the other side, 2% K_2O caused the loss of all the acid sites on VWTi catalyst and suppressed the reducibility of active vanadia species, resulting in the deactivation. As for CuNbTi catalyst, 2% K_2O also decreased the partial surface acid sites (especially strong acid sites) and declined the reducibility. However, the increase of isolated Cu^{2+} as mainly active species maintained the catalytic activity. And TiO_2 with niobium modifying would weaken the influence of potassium on NH_3 adsorption over 2% K_2O -CuNbTi catalyst. The synergistic effect between niobium species and copper species played an important role on resisting alkali poisoning. Besides, both Eley-Rideal (E-R) and Langmuir-Hinshelwood (H-L) mechanism occurred over 2% K_2O -CuNbTi at 225 °C. The adsorbed NH_3 coordinated to the Lewis acid sites and bidentate nitrate were the dominating intermediate species during the NH_3 -SCR reaction procedure over 2% K_2O -CuNbTi catalyst at 225 °C.

Acknowledgements

The authors thankfully acknowledge the financial support from the National Key Research and Development Program of China (No. 2017YFC0210904) and (No. 2017YFC0210403) and National Natural Science Foundation of China (No. 21606195).

Appendix A. Supplementary data

Supplementary material related to this article can be found, in the

online version, at doi:<https://doi.org/10.1016/j.apcatb.2019.01.049>.

References

- [1] X.S. Shang, G.R. Hu, C. He, J.P. Zhao, F.W. Zhang, Y. Xu, Y.F. Zhang, J.R. Li, J.S. Chen, Regeneration of full-scale commercial honeycomb monolith catalyst (V_2O_5 - WO_3 / TiO_2) used in coal-fired power plant, *J. Ind. Eng. Chem.* 18 (2012) 513–519.
- [2] K.P. Xie, J.W. Woo, D. Bernin, A. Kumar, K. Kamasamudram, L. Olsson, Insights into hydrothermal aging of phosphorus-poisoned Cu-SSZ-13 for NH_3 -SCR, *Appl. Catal. B* 241 (2019) 205–216.
- [3] Y. Peng, R.Y. Qu, X.Y. Zhang, J.H. Li, The relationship between structure and activity of MoO_3 - CeO_2 catalysts for NO removal: influences of acidity and reducibility, *Chem. Commun.* 49 (2013) 6215–6217.
- [4] Y. Peng, J.H. Li, W.Z. Si, J.M. Luo, Y. Wang, J. Fu, X. Li, J. Crittenden, J.M. Hao, Deactivation and regeneration of a commercial SCR catalyst: comparison with alkali metals and arsenic, *Appl. Catal. B* 168–169 (2015) 195–202.
- [5] L.J. Zhang, S.P. Cui, H.X. Guo, X.Y. Ma, X.G. Luo, The influence of K^+ cation on the MnO_x - CeO_2 / TiO_2 catalysts for selective catalytic reduction of NO_x with NH_3 at low temperature, *J. Mol. Catal. A* 390 (2014) 14–21.
- [6] L. Chen, J.H. Li, M.F. Ge, The poisoning effect of alkali metals doping over nano V_2O_5 - WO_3 / TiO_2 catalysts on selective catalytic reduction of NO_x by NH_3 , *Chem. Eng. J.* 170 (2011) 531–537.
- [7] F.S. Tang, B.L. Xu, H.H. Shi, J.H. Qiu, Y.N. Fan, The poisoning effect of Na^+ and Ca^{2+} ions doped on the V_2O_5 / TiO_2 catalysts for selective catalytic reduction of NO by NH_3 , *Appl. Catal. B* 94 (2010) 71–76.
- [8] X. Li, X.S. Li, R.T. Yang, J.S. Mo, J.H. Li, J.M. Hao, The poisoning effects of calcium on V_2O_5 - WO_3 / TiO_2 catalyst for the SCR reaction: comparison of different forms of calcium, *Mol. Catal.* 434 (2017) 16–24.
- [9] O. Kröcher, M. Elsener, Chemical deactivation of V_2O_5 - WO_3 / TiO_2 SCR catalysts by additives and impurities from fuels, lubrication oils, and urea solution, *Appl. Catal. B* 77 (2008) 215–227.
- [10] X.S. Du, X. Gao, R.Y. Qu, P.D. Ji, Z.Y. Luo, K.F. Cen, The influence of alkali metals on the Ce-Ti mixed oxide catalyst for the selective catalytic reduction of NO_x , *Chemcatchem* 4 (2012) 2075–2081.
- [11] S.S.R. Putluru, A. Riisager, R. Fehrmann, Alkali resistant Cu/zeolite de NO_x catalysts for flue gas cleaning in biomass fired applications, *Appl. Catal. B* 101 (2011) 183–188.
- [12] X.X. Wang, Y. Shi, S.J. Li, W. Li, Promotional synergistic effect of cu and nb doping on a novel Cu/Ti-Nb ternary oxide catalyst for the selective catalytic reduction of NO_x with NH_3 , *Appl. Catal. B* 220 (2018) 234–250.
- [13] G. Kresse, J. Furthmüller, Efficient iterative schemes for ab initio total-energy calculations using a plane-wave basis set, *Phys. Rev. B* 54 (1996) 11169–11186.
- [14] J.P. Perdew, K. Burke, M. Ernzerhof, Generalized gradient approximation made simple, *Phys. Rev. Lett.* 77 (1996) 3865–3868.
- [15] G. Kresse, D. Joubert, From ultrasoft pseudopotentials to the projector augmented-wave method, *Phys. Rev. B* 59 (1999) 1758–1775.
- [16] H.J. Monkhorst, J.D. Pack, Special points for brillouin-zone integrations, *Phys. Rev. B* 13 (1976) 5188–5192.
- [17] H.L. Zheng, W.Y. Song, Y. Zhou, S.C. Ma, J.L. Deng, Y.H. Li, J. Liu, Z. Zhao, Mechanistic study of selective catalytic reduction of NO_x with NH_3 over $Mn-TiO_2$: A combination of experimental and dft study, *J. Phys. Chem. C* 121 (2017) 19859–19871.
- [18] Q.C. Li, S.F. Chen, Z.Y. Liu, Q.Y. Liu, Combined effect of KCl and SO_2 on the selective catalytic reduction of NO by NH_3 over V_2O_5 / TiO_2 catalyst, *Appl. Catal. B* 164 (2015) 475–482.
- [19] W.S. Hu, X. Gao, Y.W. Deng, R.Y. Qu, C.H. Zheng, X.B. Zhu, K.F. Cen, Deactivation mechanism of arsenic and resistance effect of SO_4^{2-} on commercial catalysts for selective catalytic reduction of NO_x with NH_3 , *Chem. Eng. J.* 293 (2016) 118–128.
- [20] F.D. Liu, K. Asakura, H. He, W.P. Shan, X.Y. Shi, C.B. Zhang, Influence of sulfation on iron titanate catalyst for the selective catalytic reduction of NO_x with NH_3 , *Appl. Catal. B* 103 (2011) 369–377.
- [21] X.J. Yao, L. Zhang, L.L. Li, L.C. Liu, Y. Cao, X. Dong, F. Gao, Y. Deng, C.J. Tang, Z. Chen, L. Dong, Y. Chen, Investigation of the structure, acidity, and catalytic performance of $CuO/Ti_{0.95}Ce_{0.05}O_2$ catalyst for the selective catalytic reduction of NO by NH_3 at low temperature, *Appl. Catal. B* 150–151 (2014) 315–329.
- [22] Z.R. Ma, X.D. Wu, Z.C. Si, D. Weng, J. Ma, T.F. Xu, Impacts of niobia loading on active sites and surface acidity in NbO_x - CeO_2 - ZrO_2 NH_3 -SCR catalysts, *Appl. Catal. B* 179 (2015) 380–394.
- [23] P.L. Wang, S. Chen, S. Gao, J.Y. Zhang, H.Q. Wang, Z.B. Wu, Niobium oxide confined by ceria nanotubes as a novel SCR catalyst with excellent resistance to potassium, phosphorus, and lead, *Appl. Catal. B* 231 (2018) 299–309.
- [24] J.X. Yu, Z.Q. Chen, L. Zeng, Y.Y. Ma, Z. Feng, Y. Wu, H.J. Lin, L.H. Zhao, Y.M. He, Synthesis of carbon-doped $KNbO_3$ photocatalyst with excellent performance for photocatalytic hydrogen production, *Sol. Energy Mater. Sol. Cells* 179 (2018) 45–56.
- [25] D. Ye, R.Y. Qu, C.H. Zheng, K.F. Cen, X. Gao, Mechanistic investigation of enhanced reactivity of NH_4HSO_4 and NO on Nb- and Sb-doped VW/Ti SCR catalysts, *Appl. Catal. A* 549 (2018) 310–319.
- [26] S. Ali, L.Q. Chen, Z.B. Li, T.R. Zhang, R. Li, Su.H. Bakhtiar, X.S. Leng, F.L. Yuan, X.Y. Niu, Y.J. Zhu, Cu_x - $Nb_{1.1-x}$ ($x = 0.45, 0.35, 0.25, 0.15$) bimetal oxides catalysts for the low temperature selective catalytic reduction of NO with NH_3 , *Appl. Catal. B* 236 (2018) 25–35.
- [27] X.J. Yao, Q. Yu, Z.Y. Ji, Y.Y. Lv, Y.Y. Cao, C.J. Tang, F. Gao, L. Dong, Y. Chen, A comparative study of different doped metal cations on the reduction, adsorption

and activity of $\text{CuO}/\text{Ce}_{0.67}\text{M}_{0.33}\text{O}_2$ ($\text{M} = \text{Zr}^{4+}, \text{Sn}^{4+}, \text{Ti}^{4+}$) catalysts for $\text{NO} + \text{CO}$ reaction, *Appl. Catal. B* 130–131 (2013) 293–304.

[28] C.Z. Sun, J. Zhu, Y.Y. Lv, L. Qi, B. Liu, F. Gao, K.Q. Sun, L. Dong, Y. Chen, Dispersion, reduction and catalytic performance of CuO supported on ZrO_2 -doped TiO_2 for NO removal by CO , *Appl. Catal. B* 103 (2011) 206–220.

[29] Y. Peng, C.Z. Wang, J.H. Li, Structure–activity relationship of VO_x/CeO_2 nanorod for NO removal with ammonia, *Appl. Catal. B* 144 (2014) 538–546.

[30] R.Y. Qu, X. Gao, K.F. Cen, J.H. Li, Relationship between structure and performance of a novel cerium–niobium binary oxide catalyst for selective catalytic reduction of NO with NH_3 , *Appl. Catal. B* 142–143 (2013) 290–297.

[31] Z.M. Liu, S.X. Zhang, J.H. Li, J.Z. Zhu, L.L. Ma, Novel $\text{V}_2\text{O}_5\text{--CeO}_2/\text{TiO}_2$ catalyst with low vanadium loading for the selective catalytic reduction of NO_x by NH_3 , *Appl. Catal. B* 158–159 (2014) 11–19.

[32] W.S. Hu, Y.H. Zhang, S.J. Liu, C.H. Zheng, X. Gao, I. Nova, E. Tronconi, Improvement in activity and alkali resistance of a novel $\text{V}\text{--Ce}(\text{SO}_4)_2\text{--Ti}$ catalyst for selective catalytic reduction of NO with NH_3 , *Appl. Catal. B* 206 (2017) 449–460.

[33] N. Russo, D. Fino, G. Saracco, V. Specchia, Studies on the redox properties of chromite perovskite catalysts for soot combustion, *J. Catal.* 229 (2005) 459–469.

[34] J.C. Dupin, D. Gonbeau, P. Vinatier, A. Levasseur, Systematic xps studies of metal oxides, hydroxides and peroxides, *Phys. Chem. Chem. Phys.* 2 (2000) 1319–1324.

[35] D. Nicosia, I. Czekaj, O. Kröcher, Chemical deactivation of $\text{V}_2\text{O}_5/\text{WO}_3\text{--TiO}_2$ SCR catalysts by additives and impurities from fuels, lubrication oils and urea solution, *Appl. Catal. B* 77 (2008) 228–236.

[36] L. Chen, J.H. Li, M.F. Ge, The poisoning effect of alkali metals doping over nano $\text{V}_2\text{O}_5\text{--WO}_3/\text{TiO}_2$ catalysts on selective catalytic reduction of NO_x by NH_3 , *Chem. Eng. J.* 170 (2011) 531–537.

[37] Z. Chen, C. Fan, L. Pang, S.J. Ming, P. Liu, T. Li, The influence of phosphorus on the catalytic properties, durability, sulfur resistance and kinetics of $\text{Cu}\text{--SSZ-13}$ for NO reduction by $\text{NH}_3\text{-SCR}$, *Appl. Catal. B* 237 (2018) 116–127.

[38] D.H. Jo, G.T. Park, T.Y. Ryu, S.B. Hong, Economical synthesis of high-silica LTA zeolites: a step forward in developing a new commercial $\text{NH}_3\text{-SCR}$ catalyst, *Appl. Catal. B* 243 (2019) 212–219.

[39] N.Y. Topsøe, H. Topsøe, J.A. Dumesic, Vanadia/titania catalysts for selective catalytic reduction (SCR) of nitric-oxide by ammonia. I. Combined temperature-programmed in-situ FTIR and on-line mass-spectroscopy studies, *J. Catal.* 151 (1995) 226–240.

[40] L. Zhang, L.L. Shi, L. Huang, J.P. Zhang, R.H. Gao, D.S. Zhang, Rational design of high-performance deNO_x catalysts based on $\text{Mn}_x\text{Co}_{3-x}\text{O}_4$ nanocages derived from metal-organic frameworks, *ACS Catal.* 4 (2014) 1753–1763.

[41] M.A. Centeno, I. Carrizosa, J.A. Odriozola, $\text{NO}\text{--NH}_3$ coadsorption on vanadia/titania catalysts: Determination of the reduction degree of vanadium, *Appl. Catal. B* 29 (2001) 307–314.

[42] O.M. Busch, W. Brijoux, S. Thomson, F. Schüth, Spatially resolving infrared spectroscopy for parallelized characterization of acid sites of catalysts via pyridine sorption: possibilities and limitations, *J. Catal.* 222 (2004) 174–179.

[43] D. Delimaris, T. Ioannides, VOC oxidation over $\text{CuO}\text{--CeO}_2$ catalysts prepared by a combustion method, *Appl. Catal. B* 89 (2009) 295–302.

[44] X. Li, X.S. Li, J.J. Chen, J.H. Li, J.M. Hao, An efficient novel regeneration method for Ca-poisoning $\text{V}_2\text{O}_5\text{--WO}_3\text{--TiO}_2$ catalyst, *Catal. Commun.* 87 (2016) 45–48.

[45] B. Coq, D. Tachon, F. Figueiras, G. Mabilon, M. Prigent, Selective catalytic reduction of nitrogen monoxide by decane on copper-exchanged mordenites, *Appl. Catal. B* 6 (1995) 271–289.

[46] S. Kieger, G. Delahay, B. Coq, B. Neveu, Selective catalytic reduction of nitric oxide by ammonia over Cu-FAU catalysts in oxygen-rich atmosphere, *J. Catal.* 183 (1999) 267–280.

[47] P.G.W.A. Kompio, A. Brückner, F. Hippler, G. Auer, E. Löffler, W. Grüner, A new view on the relations between tungsten and vanadium in $\text{V}_2\text{O}_5\text{--WO}_3\text{--TiO}_2$ catalysts for the selective reduction of NO with NH_3 , *J. Catal.* 286 (2012) 237–247.

[48] N.Y. Topsøe, Mechanism of the selective catalytic reduction of nitric oxide by ammonia elucidated by in situ on-line fourier transform infrared spectroscopy, *Science* 265 (1994) 1217–1219.

[49] M.P. Ruggeri, I. Nova, E. Tronconi, J.A. Pihl, T.J. Toops, W.P. Partridge, In-situ DRIFTS measurements for the mechanistic study of NO oxidation over a commercial Cu-CHA catalyst, *Appl. Catal. B* 166–167 (2015) 181–192.

[50] L. Ma, J.H. Li, R. Ke, L.X. Fu, Catalytic performance, characterization, and mechanism study of $\text{Fe}_2(\text{SO}_4)_3\text{--TiO}_2$ catalyst for selective catalytic reduction of NO_x by ammonia, *J. Phys. Chem. C* 115 (2011) 7603–7612.

[51] A.L. Kustov, M.Y. Kustova, R. Fehrmann, P. Simonsen, Vanadia on sulphated- ZrO_2 , a promising catalyst for NO abatement with ammonia in alkali containing flue gases, *Appl. Catal. B* 58 (2005) 97–104.

[52] L. Wei, S.P. Cui, H.X. Guo, L.J. Zhang, The effect of alkali metal over Mn/TiO_2 for low-temperature SCR of NO with NH_3 through DRIFTS and DFT, *Comp. Mater. Sci.* 144 (2018) 216–222.

[53] L. Shi, T. Yu, X.Q. Wang, J. Wang, M.Q. Shen, Properties and roles of adsorbed NH_3 and NO_x over Cu/SAPO-34 zeolite catalyst in $\text{NH}_3\text{-SCR}$ process, *Wuli Huaxue Xuebao/ Acta Physico-Chimica Sinica* 29 (2013) 1550–1557.

[54] M. Calatayud, C. Minot, Effect of alkali doping on a $\text{V}_2\text{O}_5\text{--TiO}_2$ catalyst from periodic DFT calculations, *J. Phys. Chem. C* 111 (2007) 6411–6417.

[55] J.P. Chen, R.T. Yang, Mechanism of poisoning of the $\text{V}_2\text{O}_5\text{--TiO}_2$ catalyst for the reduction of NO by NH_3 , *J. Catal.* 125 (1990) 411–420.

[56] P.P. Hu, Z.W. Huang, X. Gu, F. Xu, J.Y. Gao, Y. Wang, Y.X. Chen, X.F. Tang, Alkali-resistant mechanism of a hollandite deNO_x catalyst, *Environ. Sci. Technol.* 49 (2015) 7042–7047.

Update

Applied Catalysis B: Environmental

Volume 271, Issue , 15 August 2020, Page

DOI: <https://doi.org/10.1016/j.apcatb.2019.03.018>



Corrigendum

Corrigendum to “The alkali resistance of CuNbTi catalyst for selective reduction of NO by NH₃: A comparative investigation with VWTi catalyst” [Appl. Catal. B: Environ. 246 (2019) 166–179]



Xiaoxiang Wang^a, Qiliang Cong^a, Liang Chen^a, Yun Shi^b, Yao Shi^a, Sujing Li^{a,*}, Wei Li^{a,*}

^a Key Laboratory of Biomass Chemical Engineering of Ministry of Education, Institute of Industrial Ecology and Environment, College of Chemical and Biological Engineering, Zhejiang University, Hangzhou 310027, China

^b Zhejiang University of Science & Technology, Hangzhou 310023, China

The authors regret to inform that figures and figure caption were wrongly published in the original article. Revised figures and caption are provided below:

(1) Figure 1 in the original manuscript should be revised as below. (There lacked Fig. 1(c) and (d) in the final edition.)

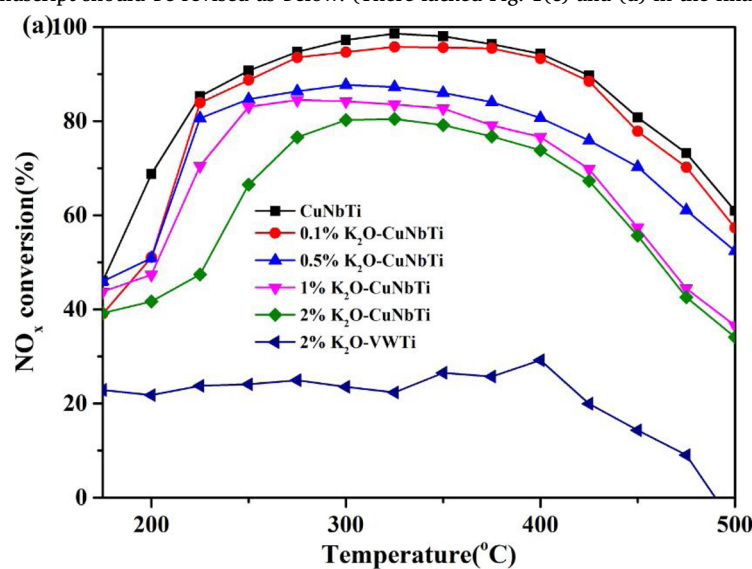


Fig. 1 NO_x conversion and N₂ selectivity over: (a)–(b) different mass ratios of K₂O-loaded CuNbTi and VWTi catalysts and (c)–(d) different alkalis poisoning CuNbTi catalysts. Reaction conditions: [NH₃] = [NO_x] = 500 ppm, [O₂] = 5%, [H₂O] = 5%, total flow rate = 500 mL min⁻¹, GHSV = 177,000 h⁻¹ and N₂ as balance.

(2) “O 1 s” should be revised to “O 1s” in the caption of Fig. 3.

(3) Figure 8 should be revised as below.

DOI of original article: <https://doi.org/10.1016/j.apcatb.2019.01.049>

* Corresponding authors.

E-mail addresses: sujing-li@zju.edu.cn (S. Li), w_li@zju.edu.cn (W. Li).

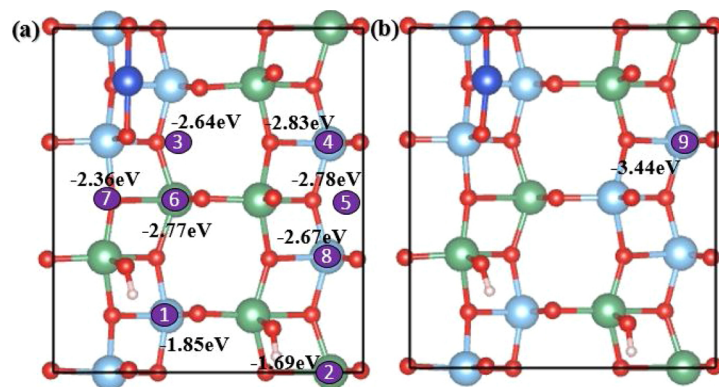


Fig. 8 (a)–(b) Possible sites for K locating at CuNbTi models and (c)–(d) the binding energy of K bonded with Nb=O, Nb–OH, Ti=O, and Ti–OH. ● represented Ti atom, ● represented Nb atom, ● represented Cu atom, ● represented H atom, ● represented O atom and ● represented the possible locating sites for K atoms.

The authors would like to apologise for any inconvenience caused.